

THESIS FOR THE DEGREE OF DOCTOR OF PHILOSOPHY

**Polyethylene Blends, a Material Concept for Future HVDC-cable Insulation**

MATTIAS ANDERSSON



Department of Chemistry and Chemical Engineering

CHALMERS UNIVERSITY OF TECHNOLOGY

Gothenburg, Sweden 2017

**POLYETHYLENE BLENDS, A MATERIAL CONCEPT FOR FUTURE HVDC-CABLE  
INSULATION**

MATTIAS ANDERSSON

© MATTIAS ANDERSSON, 2017.

ISBN 978-91-7597-541-2

Doktorsavhandlingar vid Chalmers Tekniska Högskola

Ny serie nr 4222

ISSN 0346-718X

Department of Chemistry and Chemical Engineering

Chalmers University of Technology

SE-412 96 Gothenburg

Sweden

Telephone + 46 (0)31-772 1000

Cover: Illustration of a high-voltage cable and SEM images of LDPE and a blend with 5wt% HDPE. The illustrations are done with help from Johnas Eklöf.

Chalmers Reproservice

Gothenburg, Sweden 2017

# Polyethylene Blends, a Material Concept for Future HVDC-cable Insulation

MATTTIAS ANDERSSON

Department of Chemistry and Chemical Engineering  
Chalmers University of Technology Gothenburg, Sweden

## Abstract

---

High-voltage cables are a critical component of tomorrow's power grids that seamlessly integrate hydro, wind and solar power. Further improvements in transmission capacity of both high-voltage alternating- and direct-current, HVAC and HVDC, cables are likely reached through improved insulation materials. A number of approaches to improve insulation materials are currently being considered. This thesis explores two concepts for future insulation materials: (i) polymer:metal oxide nanoparticles, and (ii) polymer:polymer blends.

To investigate the former, nanocomposites containing  $\text{Al}_2\text{O}_3$  nanoparticles dispersed in a low-density polyethylene (LDPE) matrix are considered. The addition of nanoparticles is found to improve the DC insulation properties, i.e. reduces the residual electrical conductivity, but increases the risk for electrical breakdown under AC conditions. This first part of the thesis leads to the conclusion that the use of nanocomposites can require a trade-off between AC/DC behaviour.

In the second part of this thesis polyethylene blends are investigated as an alternative to nanocomposites. The addition of minute amounts of high-density polyethylene (HDPE) to LDPE reduces the DC electrical conductivity by one order of magnitude. Moreover, trace amounts of HDPE did not appear to influence the dielectric strength under AC conditions.

Besides an improvement in electrical performance polyethylene blends display superior thermo-mechanical properties. Additive-like amounts of HDPE are able to prevent creep above the melting temperature of LDPE, which offers an alternative to crosslinking. It can be anticipated that such *thermoplastic* insulation instead of commonly used *crosslinked* polyethylene (XLPE) would considerably ease cable manufacture.

The thermo-mechanical properties are rationalised with a favourable blend microstructure. In particular, complete melt miscibility is found to give rise to a fine distribution of HDPE lamellae that, through tie chains, maintain a continuous network in molten LDPE. The extent of creep correlates with the molecular weight of HDPE.

In summary, this thesis demonstrates that the use of polyethylene blends is a promising avenue, which may lead to insulation materials with improved electrical *and* mechanical performance.

**Keywords:** *High-voltage insulation, polymer blends, nanocomposites, polyethylene, conductivity, tie-chain, thermomechanical properties*

# List of publications

The thesis is based on the following papers, referred to by roman numerals in the text.

- I. **Trade-off in AC/DC Behaviour of a Polyethylene Nanocomposite** Mattias G. Andersson, Carmen Cobo Sánchez, Tuan Anh Hoang, Linda Fogelström, Mats R. Andersson, Stanislaw Gubanski, Eva Malmström, Christian Müller. *Manuscript*
- II. **Highly insulating polyethylene blends for High-Voltage Direct-Current Power Cables**, Mattias G. Andersson, Jonna Hynynen, Mats R. Andersson, Villgot Englund, Per-Ola Hagstrand, Thomas Gkourmpis, Christian Müller. *ACS Macro Letters*, 2017, 6, 78-82
- III. **Invariant Dielectric Strength upon Addition of Low Amounts of HDPE to LDPE**, Mattias G. Andersson, Xiangrong Chen, Jonna Hynynen, Mats R. Andersson, Thomas Gkourmpis, Per-Ola Hagstrand, Stanislaw Gubanski, Christian Müller, *IEEE Conference on Electrical Insulation and Dielectric Phenomena*, 2016, 711-714
- IV. **Additive-Like Amounts of HDPE Prevent Creep of Molten LDPE: Phase-Behaviour and Thermo-Mechanical Properties of a Melt-Miscible Blend**, Mattias G. Andersson, Jonna Hynynen, Mats R. Andersson, Per-Ola Hagstrand, Thomas Gkourmpis, Christian Müller. *Journal of Polymer Science, Part B: Polymer Physics* 2017, 55, (2), 146-156
- V. **Influence of Molecular Weight on the Creep Resistance of Almost Molten Polyethylene Blends**, Mattias G. Andersson, Roman Städler, Per-Ola Hagstrand, Thomas Gkourmpis, Mats R. Andersson, Christian Müller. *Submitted*

## Contribution report

- I. Main author and responsible for data analysis. Sample preparation and data collection were carried out together with C.C.S. AC-treeing was performed together with X.C. and DC-conductivity measurements were done by T.H.
- II. Main author, sample preparation, performed thermal analysis, and SAXS. Responsible for data analysis. J.H. carried out the DC-conductivity measurements
- III. Main author, sample preparation, data collection and data analysis. Electrical treeing experiments were carried out together with X. C
- IV. Main author, sample preparation, data collection and data analysis. J.H. assisted in the sample preparation and DSC measurements. SEM images were taken together with Anders Mårtensson and J.H.
- V. Main author, all sample preparation, data collection and all data analysis.

## Related publications, not included in thesis

**Dielectric strength of  $\gamma$ -radiation crosslinked, high vinyl-content polyethylene**, Mattias G. Andersson, Markus Jarvid, Anette Johansson, Stanislaw Gubanski, Mark Foreman, Christian Müller, Mats R. Andersson. *European Polymer Journal*, 2014, 64, 101-107

**AC and DC Pre-stressed Electrical Trees in LDPE and its Aluminium Oxide Nanocomposite**, Xiangrong Chen, Deni Murdany, Dongming Liu, Mattias G. Andersson, Stanislaw M. Gubanski, Ulf W. Gedde, Suwarno. *IEEE Transaction on Dielectrics and Electrical Insulation*, 2016, 23, (3), 1506-1514



# Table of contents

|  |           |
|--|-----------|
| <b>1. Aim of project</b> .....   | <b>1</b>  |
| <b>2. Introduction</b> .....   | <b>3</b>  |
| <b>3. High-voltage cables</b> .....  | <b>5</b>  |
| <b>4. Polyethylene</b> .....   | <b>9</b>  |
| 4.1 <i>Polyethylene as an insulation material</i> .....                                    | 14        |
| <b>5. Nanocomposites</b> .....   | <b>17</b> |
| <b>6. Polymer blends</b> .....   | <b>21</b> |
| <b>7. Materials and methods</b> .....  | <b>25</b> |
| 7.1 <i>Materials</i> .....   | 26        |
| 7.2 <i>Electrical characterisation</i> .....   | 26        |
| 7.3 <i>Micro and nanostructure analysis</i> .....  | 27        |
| 7.4 <i>Mechanical testing</i> .....  | 27        |
| <b>8. Nanocomposites with Al<sub>2</sub>O<sub>3</sub> nanoparticles</b> .....              | <b>29</b> |
| 8.1 <i>Functionalisation of nanoparticles with a thioxanthone voltage stabiliser</i> ..... | 31        |
| <b>9. LDPE/HDPE blends</b> .....   | <b>37</b> |
| 9.1 <i>Co-crystallisation</i> .....  | 37        |
| 9.2 <i>Phase diagram</i> .....   | 40        |
| 9.3 <i>Diffusion of HDPE into LDPE confirms miscibility</i> .....                          | 41        |
| 9.4 <i>Distribution of crystal lamellae</i> .....  | 42        |
| 9.5 <i>Impact of HDPE on blend nanostructure</i> .....                                     | 45        |
| 9.6 <i>DC-conductivity of LDPE/HDPE blends</i> .....                                       | 46        |
| 9.6.1 <i>Thermoplastic blends</i> .....  | 46        |
| 9.6.2 <i>Crosslinked blends</i> .....  | 47        |
| 9.7 <i>AC-breakdown of crosslinked LDPE/HDPE blends</i> .....                              | 50        |
| 9.8 <i>Mechanical properties</i> .....   | 51        |
| <b>10. Conclusions</b> .....   | <b>59</b> |
| <b>11. The Future of insulation materials, author's thoughts</b> .....                     | <b>61</b> |
| <b>12. Acknowledgements</b> .....  | <b>63</b> |
| <b>References</b> .....  | <b>65</b> |



# 1

## **Aim of project**

---

Extruded power cables are expected to play an important role in future energy grids that will transfer energy produced in remote areas to urban centres where it will be needed. The aim of this project is to investigate the potential of novel materials concepts that will be capable to meet future demands. The cable of the future needs to be able to transfer energy more efficient than it does today. In order to achieve this goal the transmission voltage needs to be increased. An increase in voltage generates a higher electric field which leads to a number of challenges for the insulation, such as a temperature rise and increased risk of breakdown. In this project a variety of concepts are to be which have the aim to decrease the overall electrical conductivity, as well as to increase the breakdown strength and improve mechanical properties.

Currently research on high-voltage insulation materials focuses on nanocomposites and nano-dielectrics. In the first part of this thesis a nanocomposite is explored and later used as a benchmark. The conductivity and breakdown of the composite was evaluated and a voltage stabiliser was introduced to improve the breakdown strength.

In the second part a series of blends based on LDPE and HDPE were investigated. These systems can be considered as an evolution of the idea of nano-dielectrics, where the HDPE is used to alter the overall nanostructure and thereby affect the resulting electrical properties. In addition to a marked improvement of the electrical properties such a system exhibits a potential for improved thermomechanical performance due to the unique nanostructure and melt miscibility that results in the existence of a load-bearing network above the melting temperature of the LDPE base resin.



# 2

## Introduction

---

The worldwide electricity consumption has reached a staggering 24 000 TWh per year (2015) <sup>1</sup>. The same amount of energy would be sufficient to bring all of Sweden's fifteen largest lakes to a boil. Since the 1970's the production of electricity has almost quadrupled <sup>1</sup>. The majority of electric power (77%) is derived from non-renewable resources, i.e. fossil fuels including coal, oil, and natural gas, as well as nuclear energy <sup>1</sup>. In particular energy production from fossil fuels needs to be reduced in order to decrease the emission of greenhouse gases. The EU is promoting an investment in renewable energy resources and has set itself the goal to use at least 75% of renewable resources by 2050 <sup>2</sup>, which is part of its strategy to cut the emission of greenhouse gases by 80-95% by 2050. The most attractive sources of *green* energy are currently, wind, solar and hydro-electric power. Although each one of these sources of energy represents a promising alternative they share a common challenge, i.e. the remote location for energy harvesting. Wind power, for instance, is best utilised out at sea, where wind is stronger and more reliable <sup>3</sup>. Harvesting of solar power is most effective in deserts where the highest amount of solar radiation is found <sup>4,5</sup>. Instead, hydropower is often found in mountainous areas <sup>4</sup>. One solution to realise a widespread use of green power is an extensive transmission network. Some organisations such as the *Claverton Energy Group* and the *Desertec Foundation* have formulated a vision for a future pan-European super grid<sup>3,6</sup>. This vision promotes a far-reaching network of transmission lines across the continent that permits to distribute the energy from renewable resources both between European countries as well as their neighbours, mostly in North Africa (**Figure 1**). To reach its goal the EU must quadruple its power transmission capacity from currently 34 GW to 127 GW by 2050<sup>7</sup>. The most cost efficient means to transport electricity is through overhead lines. However, the construction of overhead lines is not feasible when transport over sea or densely populated areas is needed or when the landscape is visually or environmentally vital. Instead, subsea or underground cables must be installed.

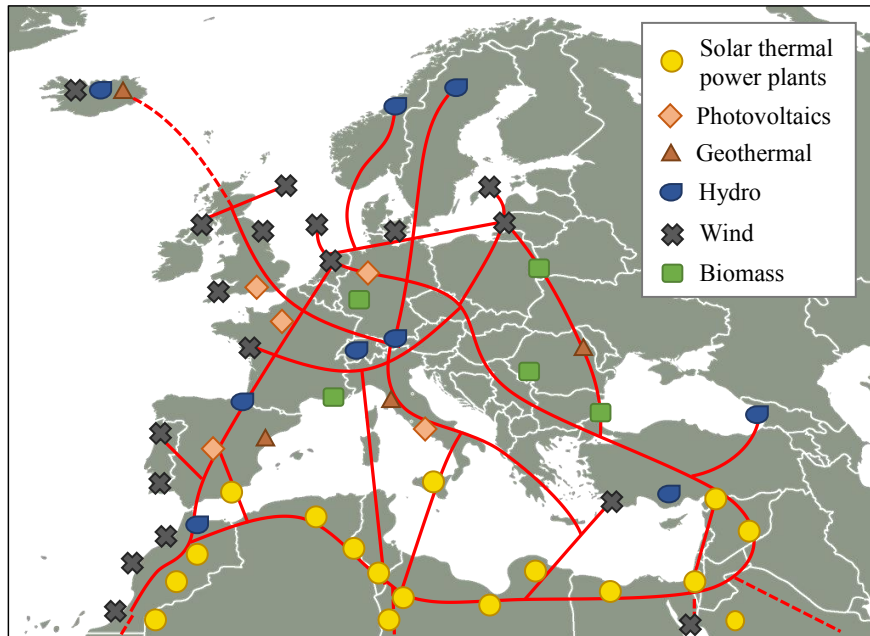


**Figure 1,** Map over Europe and northern Africa showing how a possible European/African super grid could look like.

A major difference between an underground cable and an overhead transmission line is the insulation. Whereas an overhead transmission line does not need any insulation as it is suspended in air –i.e. air acts as the insulator–an underground cable requires insulation and protection in order not to lose all current to the soil. Fabrication and installation of underground cables is more intricate and costly than that of overhead lines. It is therefore crucial that the produced power cables are of excellent quality in order to minimise the need for maintenance. One of the most important parts of a power cable is the insulation layer. Currently, considerable research efforts are dedicated to the development of new material concepts that permit further improvement of this critical component.

This thesis will provide an example for how materials research can contribute to the solving the complex task of creating a super grid, by exploring new possibilities for improved insulation materials. An improvement of the insulation material leads to more robust cables with a higher *power rating*, which means that more electrical power can be transported through a cable of a given diameter. Ultimately, fewer cables are needed to reach the same power transmission capacity, and therefore the cost associated with production, installation as well as maintenance decreases considerably. It can be anticipated that any such advance will contribute towards the realisation of a pan-European super grid that seamlessly integrates renewable sources of energy.

# 3

## High-voltage cables

---

To realise a future European super grid, power cables are essential for transport of electricity between countries, both over land and sea. High-voltage (HV) transmission networks have been used for more than a century. The first high-voltage lines were used for powering street lamps. During the late 1800s, at the time when high-voltage transmission was developed, a fierce competition arose (later known as the ‘War of the Currents’) between Thomas Edison and George Westinghouse (and Nikola Tesla). Their dispute concerned the type of current that should be used for the transport of electricity. Edison promoted the use of direct current (DC) as an effective and safe means for this purpose. Westinghouse, on the other hand, invested in an alternating current (AC) network that supplied power to street lamps. After many contests over safety issues that led to the electrocution of dogs, horses and elephants the argument was won by Westinghouse. The main advantage of AC current was the ability to easily increase and decrease the voltage through the use of transformers. AC cables were then used exclusively, until 1954, when the first large scale DC-cable was installed between the island of Gotland and the Swedish mainland. The cable had a rating of 80 kV and could transfer 20 MW<sup>8</sup>. Gotland also became the place for the world’s first extruded polymeric HVDC cable, which was laid between Bäckes and Näs in 1998 with a voltage rating of 80 kV and 50 MW<sup>9,10</sup>. The importance of HVDC cables for modern transmission grids is rapidly growing. HVDC offers superior performance for transport over long distances of more than 100 km<sup>10,11</sup>. However, HVDC is associated with high installation costs as the current needs to be inverted (from DC to AC) and rectified (from AC to DC) to be distributed. Despite a high installation cost, HVDC cables are essential for long distance transport of power from renewable energy sources, which currently are in high demand. Once the energy has been transported from the collection area to a converter station it is distributed to end users via a HVAC cable system.

## High-voltage cables

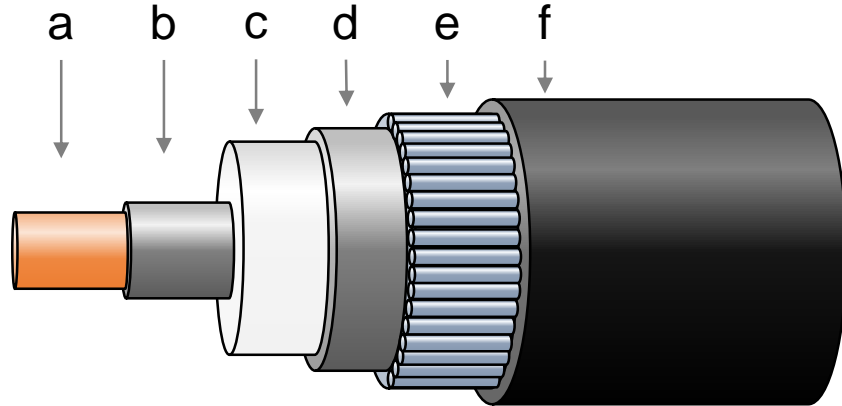


**Figure 2**, Schematic picture of a typical underground high-voltage cable: **(a)** conductor, **(b)** inner semiconducting or ‘semicon’ layer, **(c)** insulation layer, **(d)** outer semiconducting or ‘semicon’ layer, **(e)** metallic screen, and **(f)** outer sheath.

There is a variety of cables available that can be sorted into four categories according to the type of insulation, i.e. paper-oil, oil filled, polypropylene paper laminated and extruded polymer<sup>10</sup>. Currently, the majority of high-voltage cables installed around the world comprise paper-oil insulation. However, several publications argue that extruded polymer insulation is likely to represent an increasing share of the market because of benefits such as a higher operating temperature, cost-effective manufacture, light weight and reduced maintenance<sup>12-14</sup>. A typical polymeric high-voltage cable consists of a conducting core made out of aluminium or copper. Around the core an inner semiconducting layer is applied that is typically made of a carbon black filled crosslinked polyethylene (XLPE) (**Figure 2**). This ‘semicon’ layer allows for a homogenous distribution of the electric field, which emanates from the conducting core, and facilitates good contact between the conductor and the insulation layer. The insulation layer typically consist of XLPE and is the most crucial layer in a cable as it prevents current leakage to the surroundings. The insulation is surrounded by the outer semiconducting layer, which also consists of carbon black filled XLPE. The purpose of this layer is similar to that of the inner ‘semicon’ layer. It facilitates good electrical contact between the insulation layer and the next layer which is the metallic screen. In addition, the outer ‘semicon’ layer helps to achieve a homogeneous electric field, which deceases the risk of partial discharges and thermal runaway. The metallic screening layer is a grounded layer that helps to control the shape of the electric field and provides the cable with additional mechanical strength. The final layer is the protective sheath or jacketing that protects the cable from stresses imposed by the surroundings and commonly consists of PE. The here described architecture is

typical for underground cables on land. Subsea cables feature two additional layers. A layer composed of a lead alloy, which is often used instead of a screening layer, protects from water. The second layer is an armour of steel wires inside the jacketing that enhances the mechanical robustness, which is important when installing the cable. Further, the armour protects the cable from any external stress that may arise at the bottom of the sea.

The performance of a cable can be measured by the amount of power ( $P$ ) that can be transferred, and is given by  $P = I \times V$ , where  $I$  is the current and  $V$  is the voltage<sup>11, 15</sup>. To maximise the power either voltage or current can be increased. However, a high current would lead to significant heat losses through Joule heating since  $P_{loss} \propto I^2$ <sup>15</sup>. In order to minimise heat losses the voltage is increased instead. However, a high voltage enhances the electrical stress experienced by the insulation, which is different in case of HVDC and HVAC cables. With regard to HVDC insulation the electrical stress is primarily governed by the electrical conductivity ( $\sigma$ ) of the insulation. The conductivity plays an important part in the build-up of space charge, i.e. localised charges that are trapped in the insulation material. Space charges can distort and locally enhance the electric field, which increases the risk of electrical breakdown<sup>16-19</sup>. Any residual electric current also contributes to heat generation in the cable insulation. The temperature difference across the insulation is related to the electric field ( $E$ ) and electrical conductivity according to  $\Delta T \propto \sigma E^2$ <sup>10</sup>. Any increase in temperature further increases the electrical conductivity, which can lead to a self-reinforcing process in the form of thermal runaway<sup>20</sup>. In order to avoid this kind of failure mechanisms while maintaining a high-voltage rating the conductivity of the insulation needs to be decreased significantly. Currently, the highest voltage rating for a single HVDC cable with extruded XLPE insulation is ~525 kV, which can transfer about ~2600 MW of power<sup>21</sup>. Elforsk, which is a Swedish research and development company, envisions a 1000 kV cable system by 2030. The Swedish industry together with several universities has formulated a developed agenda called ‘The one megavolt challenge’<sup>22</sup>. A one Megavolt cable would be able to transfer up to 5000 MW over a distance of 2000 km, which roughly corresponds to the distance between Göteborg and Barcelona.

HVAC insulation does not suffer from charge build-up and therefore the risk of thermal runaway is minimal. However, the alternating current encourages other breakdown mechanisms such as electrical treeing<sup>23</sup>. Electrical trees consist of electrically conducting gas-filled voids that resembles the structure of a tree, with stem and branches<sup>24-28</sup> (**Figure 3**). This type of breakdown is caused by electrons that are accelerated in an electric field and reach a high enough energy to cause impact ionisation, which can lead to scission of a polyethylene chain<sup>24</sup>. This process can result in the formation of voids that will sustain partial discharges once they reach a certain size. This in turn will initiate the growth of electrical trees through repeating partial discharges. An electrical tree can grow radially through an entire layer of insulation material causing complete electrical breakdown of the cable. Electrical trees often initiate from defects in the insulation material or protrusions from the conductor where the electric field is enhanced. The probability of treeing in XLPE insulation can be mitigated through the use of an ultra-clean PE resin that contains a minimal amount of impurities. However, as voltage ratings are increasing the ultra-clean PE approach ceases to be sufficient to counter electrical tree formation<sup>29,30</sup>. In order to further decrease the risk of electrical breakdown, additives called voltage stabilisers or tree retarders can be used. These additives capture high energy electrons and reduce their energy to a level below the energy needed for impact ionisation. The voltage stabiliser concept was first introduced in a series of patents by the *Simplex Wire and Cable Company*, which was followed up by a larger study by Ashcraft et al.<sup>31</sup>. Since then a number of suitable compounds such as polycyclic aromatics<sup>31</sup>, aromatic dyes<sup>32</sup>, benzophenones<sup>33</sup>, thioxanthenes<sup>34</sup>, fullerenes<sup>35</sup>, and peroxide decomposition products (acetophenone, cumyl alcohol) have been identified<sup>36,37</sup>. Jarvid et al. have singled out a high electron affinity as a requirement for a high stabilising efficacy<sup>38</sup>.



**Figure 3**, Electrical trees in polyethylene grown from a 10 µm thick wire.

# 4

## Polyethylene

---

Polyethylene (PE) is the most prominent synthetic polymer. It is used for a variety of applications from shopping bags and packaging to bone implants and high-voltage cables <sup>39</sup>. It consists of the repeating unit  $-\text{CH}_2-\text{CH}_2-$  and was first synthesised by accident in 1933 by Reginald Gibson and Eric Fawcett who worked at the Imperial Chemical Industries (ICI) in England <sup>40</sup>. The polyethylene produced was a low-density polyethylene (LDPE). At the time industrial impact was low because the synthesis of LDPE demands high temperatures and high pressure, which is difficult to control. However, polyethylene certainly contributed to the Allied war effort during World War II in the form of cable insulation for radar systems on board of Royal Air Force (RAF) planes. In the 1950s Giulio Natta and Karl Ziegler discovered a titanium based catalyst that made it possible to produce polyethylene at atmospheric pressure and at more practical temperatures (70-90 °C). The polyethylene produced was a high-density polyethylene (HDPE). The discovery led to the large scale industrial production of polyethylene, which in 1963 earned Ziegler and Natta the Nobel prize in chemistry. Today high pressure synthesis and catalysed polymerisation routes are used commercially for the production of branched and linear polyethylene, respectively.

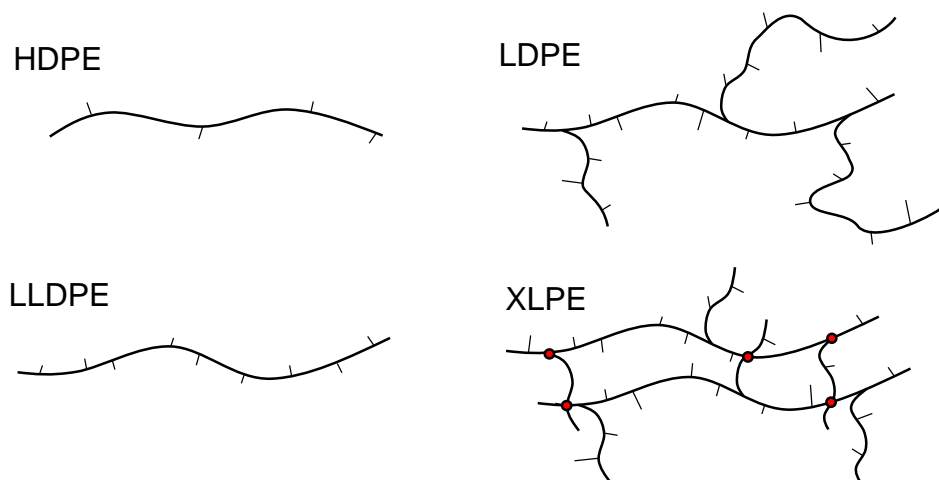


**Figure 4**, Schematic structure of different polyethylene grades. High-density polyethylene (HDPE), low-density polyethylene (LDPE), linear low-density polyethylene (LLDPE) and crosslinked polyethylene (XLPE).

Even though the repeating unit of polyethylene is simple a number of chain configurations exist that lend the possibility to produce a wide range of materials with different properties. The three most common grades of polyethylene are low-density polyethylene (LDPE), high-density polyethylene (HDPE) and linear low-density polyethylene (LLDPE) (**Figure 4**). The difference in density originates from the degree of branching in the polymer chain. HDPE is the linear form with no long chain branches (LCBs), i.e. branches that are longer than the average critical entanglement length ( $\sim 1 \text{ kg mol}^{-1}$ )<sup>41</sup>, and only a few short chain branches (SCBs; not more than 2 per 1000 carbons), which are typically in the range between a methyl and butyl group<sup>42, 43</sup>. The linear structure of HDPE facilitates a solid-state nanostructure that is characterised by a high degree of order with a crystallinity of up to 80% and a density of  $\rho_{HDPE} \sim 0.94$  to  $0.97 \text{ kg m}^{-3}$ <sup>44</sup>. LDPE consist of both LCBs (1-2 per 1000 carbons) and SCBs (10-50 per 1000 carbons)<sup>45, 46</sup>, which dramatically changes the property of the material. SCBs hinder the chain from forming thick crystals as branching points represent defects that cannot be a part of an ordered domain. This leads to a less ordered material with a crystallinity of 30-55% and a lower density of  $\rho_{LDPE} \sim 0.91$  to  $0.94 \text{ kg m}^{-3}$ .

One significant difference between LDPE and HDPE is the melting behaviour. LDPE tends to feature a broad distribution of crystal sizes and therefore a broad melting endotherm with an onset as low as  $0^\circ\text{C}$  and a peak around  $100\text{-}110^\circ\text{C}$ . Instead, the melting endotherm of HDPE is much narrower with a peak above  $130^\circ\text{C}$  (**Figure 5**).

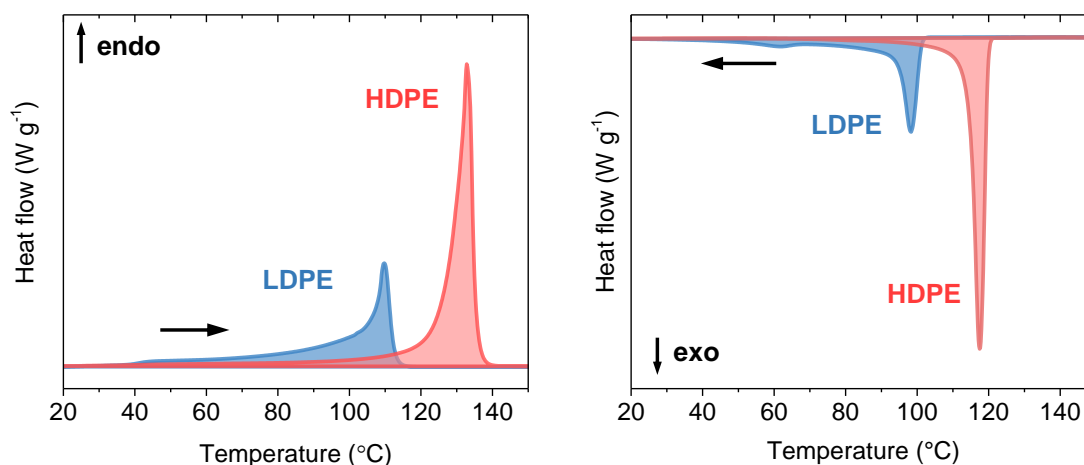


**Figure 5**, Differential scanning calorimetry (DSC) heating and cooling thermograms showing the melting endotherm (**left**) and crystallisation exotherm (**right**) of LDPE and HDPE.

## Polyethylene

Solidification of polyethylene from the melt leads to the formation of crystalline lamellae that are separated by amorphous regions (**Figure 6**). The lamellar thickness is on the order of ten nanometres. Polymer chains, which tend to be considerably longer, can either fold to re-enter the same lamella or transverse the amorphous region to join an adjacent lamella. On a micrometre scale lamellae can arrange themselves into sphere-like structures, so-called spherulites, or sheaf-like structures, so-called axialites<sup>47</sup>. Crystallisation starts with the formation of a nucleus which resides at the centre of a spherulite or axialite. Homogenous nucleation can occur spontaneously from the melt but is less common since a large degree of undercooling of 50-100 °C below the equilibrium temperature  $T_m^0 \sim 418.6$  K is required<sup>47</sup>. Instead, heterogeneous nucleation occurs from pre-existing surfaces such as contaminants, catalyst residues or seed crystals<sup>48</sup>.

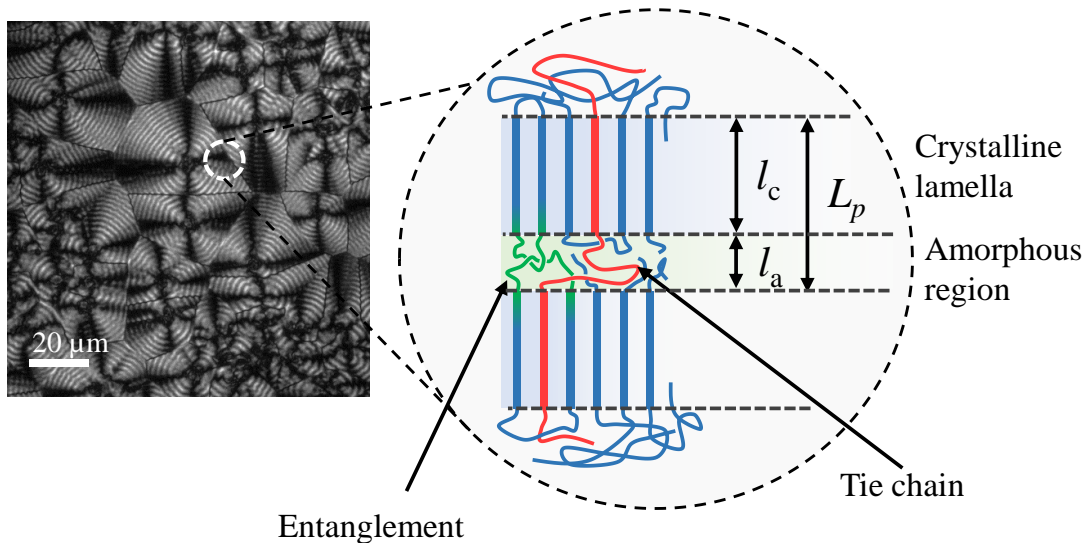


**Figure 6**, Cross-polarised optical microscopy image of a polyethylene film showing banded spherulites, and illustration of the semi-crystalline structure of polyethylene, where  $l_c$  is the lamellar thickness,  $l_a$  is the thickness of the amorphous region, and  $L_p$  is the long period.

The nano- and microstructure of polyethylene is crucial for the properties that the material will display. Therefore, to optimise a polyethylene material for a particular application it is important to elucidate relevant structure-property relationships.

To investigate the semi-crystalline structure and determine the crystallinity ( $X_c$ ) of polyethylene thermal analysis is commonly used. Differential scanning calorimetry (DSC) permits to measure

the melt enthalpy of the crystals ( $\Delta H_f$ ) that can then be compared to the melt enthalpy of 100% crystalline material ( $\Delta H_f^0$ )<sup>49</sup>.

$$X_c = \frac{\Delta H_f}{\Delta H_f^0} \quad (1)$$

Because some grades such as LDPE have a broad melting peak the temperature dependence of the heat capacity must be taken into account to calculate the correct crystallinity. This can be done by using the total enthalpy method (2) suggested by Gray et al.<sup>50</sup>:

$$X_c = \frac{\Delta H_f}{\Delta H_f^0 - \int_{T_1}^{T_2} (C_p^{amorph} - C_p^{crystal}) dT} \quad (2)$$

Where  $C_p^{amorph}$  and  $C_p^{crystal}$  are the heat capacity of the amorphous and the crystalline part, respectively.  $T_1$  and  $T_2$  are the integration limits, which also mark the temperature range used for the integration of  $\Delta H_f$ . DSC can also be used to calculate the lamellar thickness. This is done by using the correlation between the melting temperature and the thickness of crystalline lamellae as described by the Gibbs-Thomson equation:

$$l_{c,DSC} = \frac{2\sigma_e}{\Delta H_f^0} \frac{T_m^0}{T_m^0 - T_m} \quad (3)$$

where  $\sigma_e = 90.4 \text{ mJ m}^{-2}$  is the fold surface energy,  $T_m$  is the melting temperature of interest,  $T_m^0 = 418.6 \text{ K}$  denotes the equilibrium temperature of PE and  $\Delta H_f^0 = 290 \text{ MJ m}^{-3}$ <sup>51</sup>. It is common to report the peak lamellar thickness. However this value only corresponds to the most abundant lamellae and does not consider the thickness of lower or higher melting crystals.

To obtain an average lamellar thickness Small-Angle X-ray Scattering (SAXS) can be employed. SAXS probes the average repeat distance associated with (one-dimensional) stacks of alternating crystalline lamellae and amorphous regions. The long period  $L_p = 2\pi/q_p$ , where  $q_p$  is the peak scattering vector, corresponds to the sum of the average lamellar thickness and the average thickness of the amorphous region (cf. Figure 6)<sup>52</sup>. To determine the average lamellar thickness ( $l_{c,SAXS}$ ) the crystallinity calculated from DSC,  $X_c$ , can be used to determine  $l_{c,SAXS} = L_p \times X_c$ .

## Polyethylene

As described above polyethylene crystallises into stacks of crystalline lamellae separated by amorphous regions. Provided that a polymer chain is sufficiently long it can be part of more than one lamella and therefore bridge the amorphous region to create a tie chain<sup>53, 54</sup>. The number of tie chains strongly influences the fracture toughness and slow crack formation of polyethylene, which can occur when a polymer is exhibiting small stresses under long periods of time<sup>55</sup>. Tie chains distribute the load over several crystals and can therefore minimise crack formation<sup>56, 57</sup>. The probability of tie-chain formation is affected by the molecular weight, the presence of side chains, the lamellar thickness and crystallinity of the polymer. Huang and Brown have proposed a model for calculating the probability of tie-chain formation<sup>56, 57</sup>. The model is based on the molecular weight and the long period. In order for a tie chain to form it is assumed that the end-to-end distance of a polymer chain in the melt must be greater than  $2l_c + l_a$  (**Figure 7**).

$$P_M = \frac{1}{3} \left( 1 - \frac{4b^3}{\sqrt{\pi}} \int_0^L r^2 e^{-b^2 r^2} dr \right) \quad (4)$$

where  $L = 2l_c + l_a$  is the critical distance,  $b^2 = 3/2\bar{r}^2$  and  $\bar{r}$  is the end-to-end distance of a random coil of polyethylene, which is described by:

$$\bar{r} = \sqrt{(D \cdot n \cdot l^2)} \quad (5)$$

where  $D = 6.8$ ,  $n = M/14$  is the number of links and  $l = 0.153$  nm is the link distance, i.e. the bond length of a carbon-carbon bond. The Huang-Brown model implies that one of the most important factors determining the tie-chain probability is the molecular weight. An extension of the same model is able to consider the complete molecular weight distribution by averaging over all present chain lengths:

$$P = \frac{\int_0^\infty n(M) \cdot P_M dM}{\int_0^\infty n(M) dM} \quad (6)$$

where  $n(M)$  is the full molecular weight distribution and  $ndM$  is the number of molecules with a molecular weight between  $M$  and  $M + dM$ .

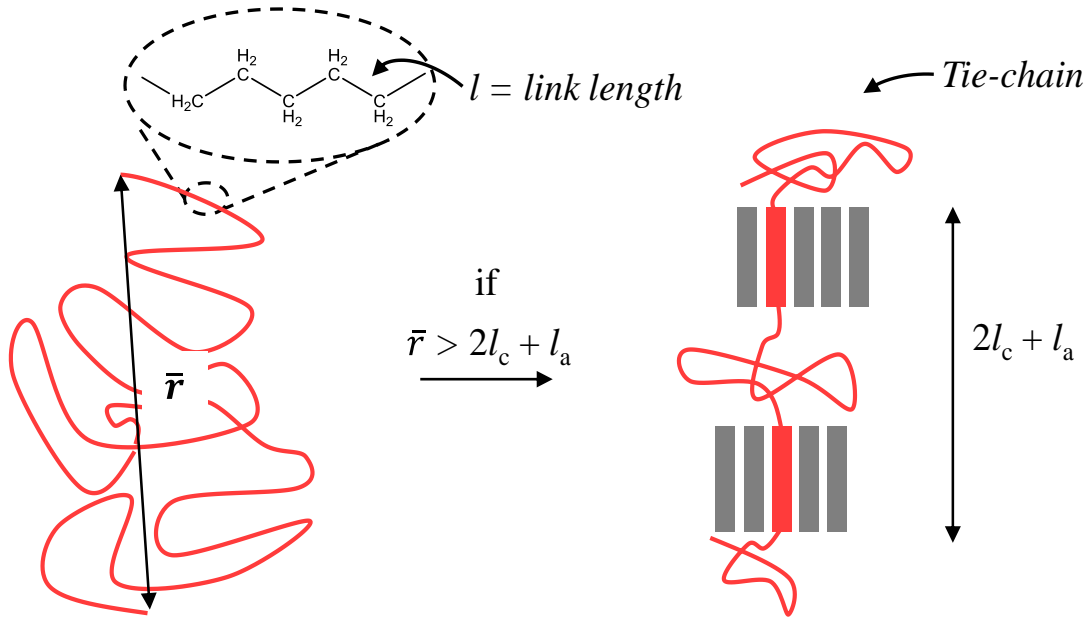


**Figure 7**, Illustration of the Huang-Brown model for the probability of tie-chain formation, where  $\bar{r}$  is the end-to-end distance and  $l_c$  and  $l_a$  are the lamellar thickness and the thickness of the amorphous region, respectively.

#### 4.1 Polyethylene as an insulation material

Polyethylene is often used as an insulation material because of its superior dielectric and mechanical properties. Moreover, polyethylene can be cost-effectively processed through e.g. extrusion and injection molding. LDPE is the preferred material solution for the insulation of high-voltage cables because of its cleanliness due to the absence of a catalyst and the architecture of the high pressure polymerisation process, which minimises the presence of contaminants. The operating temperature of a high-voltage cable can reach 90 °C, which is considerably above the onset of melting of LDPE (cf. **Figure 5**). Thus, in order to maintain the dimensional stability of the insulation crosslinking is needed. Crosslinking introduces covalent bonds between polymer chains,

which are therefore linked together to form an infusible network that improves the mechanical properties, such as creep resistance and the tensile strength at elevated temperatures <sup>58</sup>. Crosslinking can be achieved through a variety of means such as curing with peroxide <sup>59</sup>, radiation crosslinking <sup>60, 61</sup> or silane crosslinking <sup>58</sup>. The most common method used for high-voltage insulation is curing with peroxides, and the preferred compound is dicumyl peroxide (DCP). DCP is chosen because it offers a low reactivity during extrusion at 140 °C but rapid curing at around 180 °C. An amount of about 0.25% DCP is sufficient to crosslink an LDPE resin to 70 to 80% <sup>59</sup>. Crosslinking with DCP creates decomposition products such as acetophenone, cumyl alcohol,  $\alpha$ -methyl styrene and methane gas. These by-products can be harmful for both the environment and the dielectric properties of the insulation, and it is therefore necessary to remove them from the cable in a process called degassing <sup>37</sup>. The process of degassing is time consuming and can take up to several days. It is therefore a rate limiting step during the cable production process. An additional disadvantage of XLPE is the poor recyclability. After crosslinking the material cannot be melt processed anymore. This limits the use to applications where a long lifetime is required as the insulation cannot be recycled by melting.

The numerous disadvantages associated with XLPE open up the possibility to use thermoplastic alternatives instead of crosslinked insulation materials. HDPE is an obvious candidate because of its higher melting temperature and higher crystallinity. However, the residual amount of metal catalyst that likely remains present in the material may compromise the cleanliness needed for high-voltage applications. Moreover, the stiffness may cause high tension and increase the risk of stress cracking when winding the cable <sup>62, 63</sup>. An attractive approach is to use blends of HDPE and LDPE in order to combine the high melting temperature of HDPE that can provide form stability at elevated temperatures with the excellent processability of LDPE. In this thesis a variety of blends of LDPE and HDPE are explored both from an electrical and mechanical point of view.

## Polyethylene

# 5

## Nanocomposites

---

A *composite* is a “Multicomponent material comprising different (non-gaseous) phase domains in which at least one type of phase domain is a continuous phase”<sup>64</sup>. Commonly, the continuous phase is referred to as the *matrix* that encompasses the second phase or *filler*. Polymer composites are widely used because they combine a versatile processing portfolio with the possibility to create materials with superior physico-chemical properties such as a high specific strength<sup>65</sup>. A variety of materials can be introduced as fillers, including glass and carbon fibres, clay, cellulose, carbon nanotubes, graphene and metal oxides. A filler material can feature a variety of shapes and come in the form of fibres, whiskers, particles, flakes or sheets. The shape, size and orientation as well as the distribution and interaction with the matrix strongly influence the behaviour of the composite material. One key factor determining the properties of a composite is the interaction between the filler and matrix. The interaction can occur both on an atomic level through hydrogen bonds, van der Waals forces or polar interactions, and on a larger scale through surface roughness or mechanical interlocking<sup>65</sup>. All types of interactions are highly reliant on the surface area of the filler which depends on the size of the filler<sup>66</sup>. A smaller filler will offer a larger specific surface area, i.e. the surface area per mass. The influence of the interaction zone will also become more evident as the size of the filler is decreased. A composite with a filler, which has at least one dimension in the nanometre range (1-100 nm), is generally called a nanocomposite<sup>67</sup>. Nanocomposites offer a large interfacial area between the matrix and filler (**Figure 8**) and therefore tend to display a superior set of properties compared to composites comprising coarser filler materials.

In 1994 T.J. Lewis introduced the concept of using nanoscale fillers to enhance the dielectric properties of polymer insulators<sup>68</sup>. In particular nanocomposites of polyethylene and metal oxide nanoparticles such as  $\text{Al}_2\text{O}_3$ <sup>69,70</sup>,  $\text{MgO}$ <sup>71,72</sup>,  $\text{ZnO}$ <sup>73,74</sup>,  $\text{TiO}_2$ <sup>75</sup> and  $\text{SiO}_2$ <sup>76</sup> have received considerable attention because they tend to reduce the DC-conductivity. According to some reports the DC-conductivity can decrease by more than one order of magnitude upon addition of only a few weight percent of the filler material<sup>77,78</sup>.  $\text{Al}_2\text{O}_3$  and  $\text{MgO}$  have also been shown to decrease the build-up

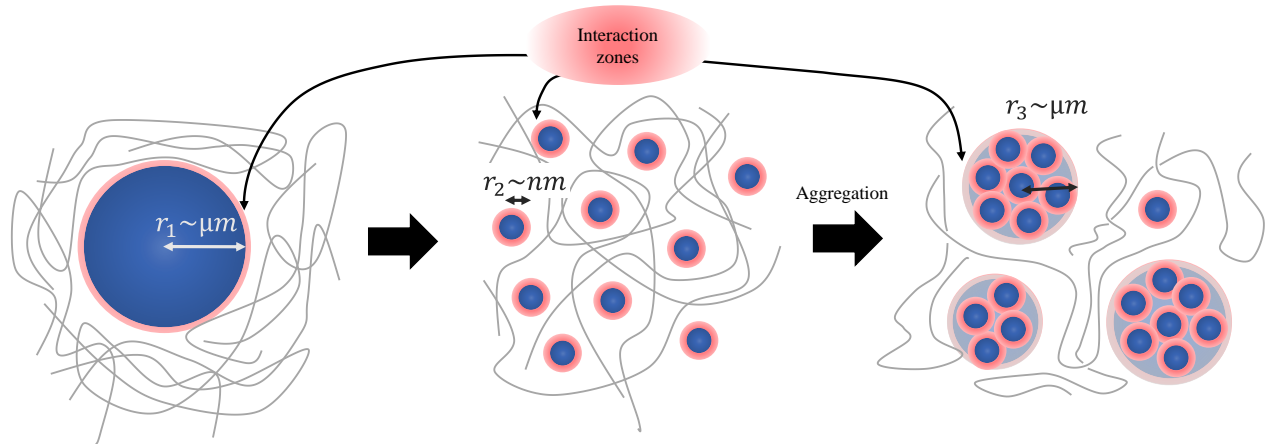


**Figure 8,** Illustration of the difference in the volume associated with the interaction zone between filler particles and the polymer matrix in case of micro- (left), nanosized particles (middle) and aggregated nanoparticles (right).

of space charge in polyethylene<sup>79-81</sup>. Several authors have proposed that charge trapping at the interface between the polymer matrix and filler gives rise to the superior dielectric properties of metal oxide nanocomposites<sup>71, 82-84</sup>. The importance of the interface has been discussed in a series of publications<sup>84-87</sup>. For instance, Tanaka et al. suggested a multicore model, which describes a number of layers outside the surface of the filler that impact both electrical and thermal properties<sup>88</sup>.

Nanoparticles are typically prepared and processed as a suspension in a liquid medium in order to avoid the formation of aggregates, which negatively impact the properties of nanocomposites<sup>89</sup>. Further, aggregation during compounding of the nanoparticles with the polymer matrix must be avoided. Aggregation would reduce the interfacial area that is available in the final composite<sup>90</sup> (**Figure 8**). Another issue to be addressed when handling metal oxide nanoparticles is the hydroxide layer that tends to cover their surface. The hydroxide layer is hydrophilic and renders the nanoparticles hygroscopic, which can result in water absorption when stored at ambient conditions. The presence of water is a concern for high-voltage applications as moisture in the insulation raises the risk for water treeing, which is a breakdown phenomenon commonly encountered in AC-cables<sup>91</sup>.

The two issues described above can be mitigated by coating the nanoparticle surface with for instance a hydrophobic layer. Coatings that don an aliphatic chain both hinder particle aggregation and render the particle surface less hydrophilic<sup>92, 93</sup>. Coating of nanoparticles has been reported to have positive effects on the electrical properties. For instance, Ma et al.<sup>75</sup> observed an improved

space charge distribution and breakdown strength when coating TiO<sub>2</sub> nanoparticles with a polar silane, although no changes in the micro- or nanostructure were found.

The superior dielectric behaviour of nanocomposites together with the possibility for a vast number of functionalisation routes holds considerable promise for the development of improved high-voltage insulation materials. However, there are drawbacks with regard to upscaling of nanocomposites. The processing of polyethylene filled with metal-oxide nanoparticles is challenging. The nanoparticles have to be homogeneously distributed in the insulation without any aggregation. Fabrication of a cable system that is thousands of kilometres long without risking any aggregation or inhomogeneous distribution of the nanoparticle filler in the insulation layer is a considerable challenge.



# 6

## Polymer blends

---

For many application areas polymer-based materials with a specific set of properties are required that cannot be satisfied by a single polymer. In such cases blending can be used to create materials that combine the properties of several polymers. A *polymer blend* is a “Macroscopically homogeneous mixture of two or more different species of polymer”<sup>94</sup>.

In the absence of crystallisation, Flory-Huggins theory can be used to describe the phase-behaviour of a two-component polymer blend<sup>95-97</sup>, which provides a simple expression for the change in Gibbs free energy upon mixing the two polymers:

$$\Delta G_{mix} = \Delta H_{mix} - T\Delta S_{mix} \quad (7)$$

The change in the enthalpy and entropy upon mixing are given by:

$$\Delta H_{mix} = Nk_B T \phi_1 \phi_2 \chi \quad (8)$$

and

$$\Delta S_{mix} = -Nk_B \left( \frac{\phi_1}{DP_1} \ln \phi_1 + \frac{\phi_2}{DP_2} \ln \phi_2 \right) \quad (9)$$

where  $\phi_1$  and  $\phi_2$  are the volume fractions of the two blend components with degrees of polymerisation  $DP_1$  and  $DP_2$ , and  $\chi(T)$  is the interaction parameter, with  $\chi > 0$  or  $\chi < 0$  in case of endothermic or exothermic mixing. Evidently, for two polymeric materials with a high molecular weight (large  $DP$ ) the entropy change is minimal, which is the reason for the poor miscibility of many polymer blends.

The compatibility of the blend components can range from miscible to immiscible, leading to either a homogeneous liquid or phase-separated domains<sup>98</sup>. Complete miscibility occurs above a certain upper critical solution temperature (UCST) where the blend exists as a homogeneous liquid (**Figure 9**). At lower temperatures the components phase-separate into two types of domains, which

are rich in one polymer that dissolves a certain amount of the other polymer and *vice versa*. Domain boundaries can be sharp or diffuse –due to the presence of a concentration gradient– and develop through binodal and spinodal decomposition, respectively <sup>47</sup>. The extent of the miscible phase

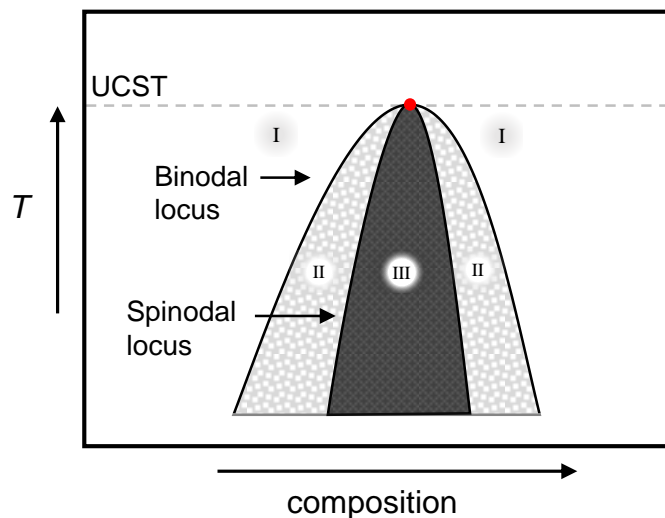


**Figure 9**, Schematic phase diagram for a blend system with polymers of similar molecular weight showing (I) a stable one-phase region, (II) the meta-stable region, and (III) an unstable region. Dashed line shows the upper critical solution temperature (UCST) with the critical point marked in red.

depends, besides the molecular weight, on the degree of interaction between the blend components in the form of van der Waals forces, dipole-dipole interactions or hydrogen bonds <sup>99</sup>. Note that the presence of hydrogen bonds can introduce a lower critical solution temperature (LCST) above which the polymer blend will phase separate <sup>100</sup>.

Upon cooling, a blend of two amorphous polymers will remain miscible, or undergo liquid-liquid phase separation, as described by Flory-Huggins theory. In case of two semi-crystalline polymers the Flory-Huggins theory only describes the phase behaviour of the molten state. Accordingly, above the melting temperature of the two components the blend can exist as either a homogeneous or phase-separated melt. Upon cooling, the two polymers *can* undergo crystallisation. Similar to liquid-liquid phase separation, the process of crystallisation leads to the formation of a heterogeneous blend nanostructure. Since both processes require diffusion of polymer chains to the growing phase-separated liquid domain or crystal growth front, respectively, in either case the solidification kinetics critically influence which type of solid-state nanostructure can develop.

If two semi-crystalline polymers phase-separate in the melt the two components will crystallise in their respective domains, with the kinetics of crystallisation influenced by the domain purity and size. Likewise, the solidification kinetics strongly impact crystallisation from a homogeneous melt. When cooled sufficiently slowly both polymers will be able to form individual crystallites. More rapid solidification can lead to the formation of co-crystals, provided that the two components are structurally similar as is the case for e.g. LDPE and HDPE. Co-crystals tend to form because a fast cooling rate prevents diffusion of polymer chains and hence crystallisation occurs predominantly with nearest-neighbour molecules, which in a miscible melt can be either blend component.

Blends of two polyolefins cover the whole spectrum from homogeneous to phase-separated melts, and pure crystal to co-crystal dominated solid-state nanostructures. For instance, chemically similar polymers such as polyethylene and polypropylene (PP) tend to phase-separate in the melt<sup>101-104</sup>. Polypropylene can be thought of as a polyethylene with regular short-chain (methyl) branches. Accordingly, a blend of two polyethylenes that feature widely different degrees of branching are immiscible<sup>105</sup>. Conversely, a more similar degree of branching can lead to partial and even complete miscibility in the melt. Many combinations of polyethylene grades (HDPE, LDPE, LLDPE) have been found to be miscible<sup>106</sup>. Melt-miscible polyethylene blends permit to tailor a wide range of properties such as their processability, toughness, strength and transparency<sup>98, 107</sup>. The phase behaviour of blends comprising LDPE and HDPE has been studied extensively by Hill et al in a series of papers, which established that the solidification behaviour is strongly influenced by molecular weight and branching<sup>108-114</sup>. Similar studies were carried out by Alamo et al who used small-angle neutron scattering (SANS) to explore the influence of branching of LLDPE on the phase behaviour of an LLDPE/HDPE blend<sup>105, 115</sup>. Phase separation in the melt was observed for a SCB frequency of more than 8 branches per 100 carbons. Although some PE systems are miscible in the melt they phase separate upon cooling into crystals of HDPE, LDPE and co-crystals (**Figure 10**). Co-crystallisation occurs if a HDPE chain is included in a LDPE crystal, or if a linear segment of a LDPE molecule is included in a HDPE crystal<sup>116, 117</sup>. The later scenario would limit the lamellar thickness and hence melting temperature of the resulting co-crystal. In case of LDPE/HDPE blends co-crystals tend to feature a lamellar thickness that lies in-between the lamellar thickness of pure LDPE and HDPE crystals, which can be observed in DSC thermograms as a third, intermediate melting endotherm<sup>118</sup>.

A number of recent studies have explored to which extent blending of LDPE and HDPE permits to modify the dielectric properties of the individual components <sup>119-124</sup>. Hosier et al <sup>120, 125</sup> reported an increase in dielectric strength by 16% upon the addition of 20% HDPE to LDPE, provided that the material was isothermally crystallised. The authors argued that the improved dielectric strength originated from a more space-filling spherulitic microstructure that could form when HDPE was able to crystallise slowly. These studies emphasise the importance of the crystallisation kinetics on the dielectric properties of polyethylene blends. Depending on the cooling rate, composition, molecular weight and branching the nano- and microstructure of the solidified blend will differ, which opens up the possibility to tailor the dielectric properties of polyethylene-based insulation materials.

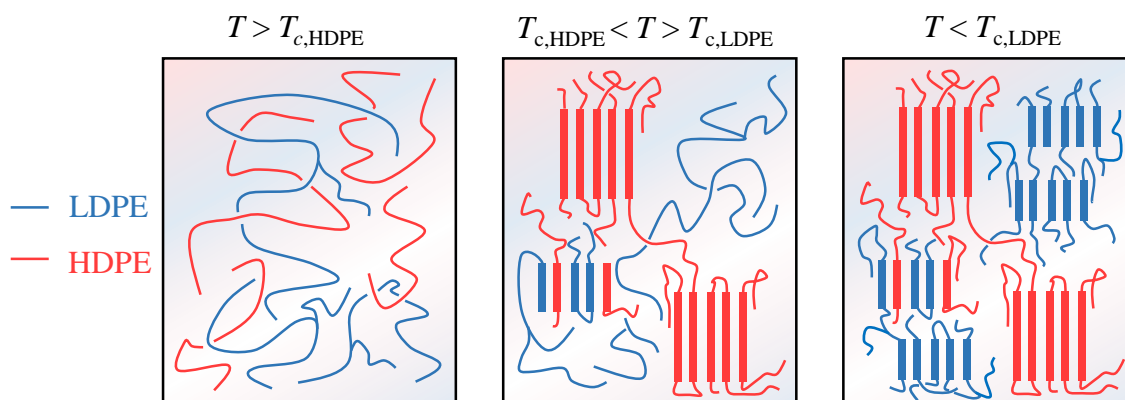


**Figure 10**, Schematic picture of the nanostructure of a melt-miscible LDPE/HDPE blend above the crystallisation temperature of both components (**left**), in-between the crystallisation temperature of both LDPE and HDPE (**centre**), and below the crystallisation temperature of both components (**right**).

# 7

## Materials and methods

This chapter contains a brief description of some of the materials and methods used in this thesis. Two types of materials were studied, metal oxide nanocomposites and polyethylene blends. **Figure 11** illustrates the experimental process for each type of material. More detailed information about the materials and experiments can be found in the respective papers.

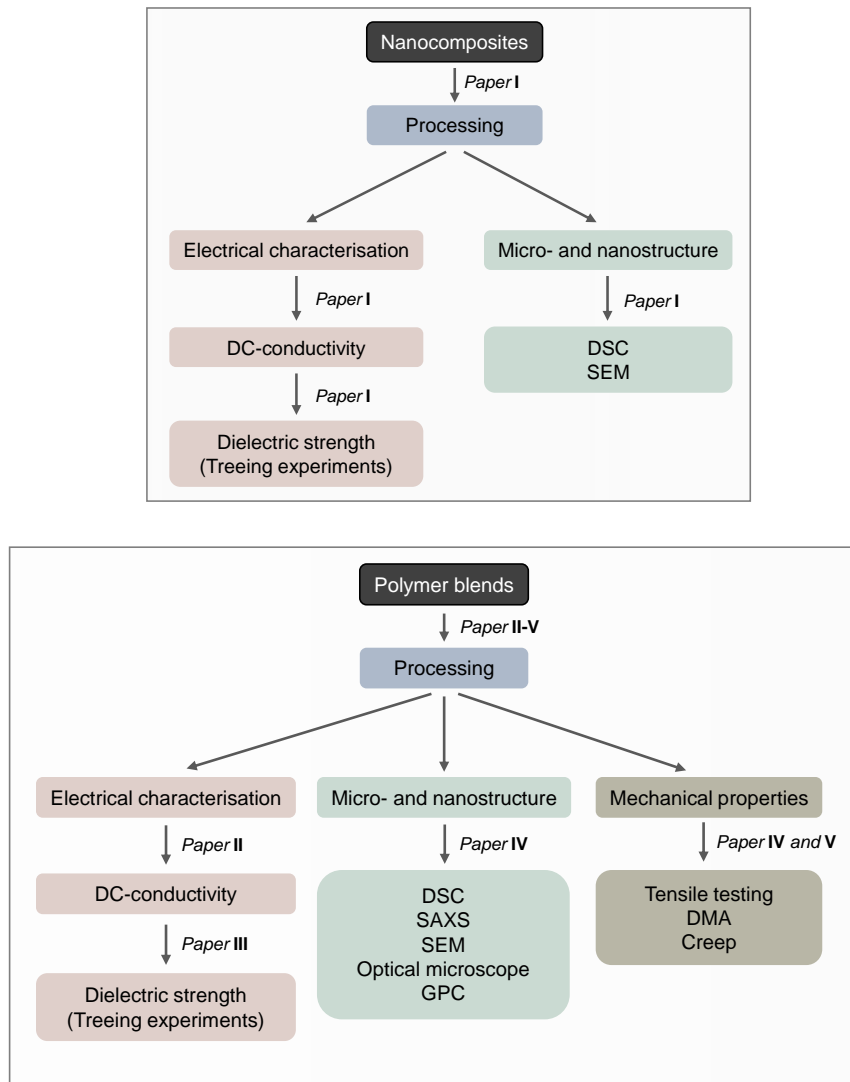


**Figure 11**, An overview of the experimental process.

## 7.1 Materials

Nanocomposites were prepared by soaking ground LDPE with a dispersion of nanoparticles for 1 hour, after which the solvent was removed. The powder was then extruded at 160 °C. Samples were finally melt pressed at 150 °C to desired shape for electrical treeing and DC-conductivity measurements.

For most polyethylene blends two grades were used: LDPE (weight-average molecular weight  $M_w^{LDPE} \sim 117 \text{ kg mol}^{-1}$ ; polydispersity index PDI  $\sim 9$ ) and HDPE ( $M_w^{HDPE} \sim 58 \text{ kg mol}^{-1}$ ; PDI  $\sim 6$ ). The LDPE branching ratio was  $n_{LCB} \sim 1.9$  per 1000 carbons. Blends with a composition ranging from 1 to 80 wt% HDPE were compounded in an extruder with a temperature gradient from 80 °C to 180 °C. Samples were then melt pressed into desired shape and cooled at  $\sim 10 \text{ °C min}^{-1}$ . Crosslinking was achieved by soaking the blends with DCP followed by melt pressing at 180 °C. To investigate the influence of molecular weight, an additional number of HDPE grades were used, ranging from 4 to 2400  $\text{kg mol}^{-1}$ . All these blends were compounded in an extruder except for 2400  $\text{kg mol}^{-1}$  which was solution blended (Paper V).

## 7.2 Electrical characterisation

Electrical characterisation included both DC-conductivity and AC electrical treeing measurements. DC-conductivity measurements were carried out both at Borealis AB, Stenungsund and in collaboration with the High-Voltage Engineering group of Stanislaw Gubanski at Chalmers. AC electrical treeing experiments were performed together with the latter. DC-conductivity was measured on 0.1 to 1 mm thick films placed between two electrodes. The desired voltage was applied and the current was measured by an electrometer. In order to control the temperature the electrodes and the sample were placed in an oven. The current was measured over time and the final conductivity was calculated when a (close to) steady current was reached.

Treeing experiments were performed at room temperature using a wire plane method. A tungsten wire with the diameter of 10  $\mu\text{m}$  was embedded between two polyethylene slabs. An aluminium tape connected to the tungsten wire was attached to the sample as the electrical contact between the high-voltage source and the wire. A 50 Hz AC voltage was applied at the tungsten wire electrode, which was increased at a rate of 22  $\text{V s}^{-1}$  (rms). The formation of electrical trees was observed in-situ with an optical microscope. For each sample the first four trees growing from non-deformed segments of the tungsten wire electrode are considered to form independent of each other

and are used for data analysis. The data were analysed using a 3-parameter Weibull distribution, which is recommended by industrial standards <sup>126</sup>.

### 7.3 Micro and nanostructure analysis

Micro- and nanostructure characterisation was carried out with DSC, SAXS, SEM and optical microscopy. DSC was performed under nitrogen between -50 to 160 °C and a heating/cooling rate of 10 °C min<sup>-1</sup>. SEM was done on cryo-fractured surfaces etched with a solution of potassium permanganate, sulfuric acid, orthophosphoric acid and water. The etched surface was gold sputtered before analysis. Optical microscopy with cross-polarised light illumination was performed on 0.1 mm thick films placed on glass slides. A heat stage was used to study diffusion behaviour with variable-temperature optical microscopy. SAXS was carried out using synchrotron radiation ( $\lambda = 0.91 \text{ \AA}$ ) at the I911-SAXS beamline of the MAX Laboratory, Lund, Sweden <sup>127</sup>. A Pilatus 1M 2D-detector placed at a distance of 1.9 m from the sample was used to record transmission SAXS patterns for 0.2 mm thick solid samples within a  $q$  range of 0.08 to 4 nm<sup>-1</sup>. Then, background-corrected 2D SAXS patterns were radially integrated and calibrated with silver behenate. Variable-temperature SAXS measurements were performed with a Linkam heat stage between room temperature and 140 °C at a heating rate of 10 °C min<sup>-1</sup>.

### 7.4 Mechanical testing

Mechanical analysis was performed by tensile testing, DMA and creep tests. DMA was carried out on 1 mm thick samples in torsion mode between 30 and 135 °C with a heating rate of 2 °C min<sup>-1</sup>. Creep experiments were done by either suspending 1 mm thick dog-bone shaped samples in a pre-heated oven at 115 °C (Paper IV), or by monitoring the creep strain at constant stress with a DMA (Paper V). In case of the latter, a stress between 1 kPa and 15 kPa was applied to the samples at a constant temperature of 115 °C.

## Materials and methods

# 8

## Nanocomposites with Al<sub>2</sub>O<sub>3</sub> nanoparticles

Nanocomposites have been shown to improve the electrical properties of PE. In this chapter a nanocomposite containing 3 wt% Al<sub>2</sub>O<sub>3</sub> is discussed. Material characterisation was done followed by conductivity and electrical breakdown measurements. In addition to naked Al<sub>2</sub>O<sub>3</sub> nanoparticles, voltage-stabiliser functionalised nanoparticles will also be discussed (**Figure 14**)

Initially, the influence of Al<sub>2</sub>O<sub>3</sub> nanoparticles on the nanostructure of LDPE was investigated because any changes are expected to affect the electrical properties. DSC indicated no significant difference between neat LDPE (PE) and LDPE containing 3wt% Al<sub>2</sub>O<sub>3</sub> (PE<sub>NP</sub>). The peak melting temperature was ~111 °C and the lamellar thickness calculated with the Gibbs-Thomson equation (eq.3) was ~7.5 nm for both materials. Likewise, the total crystallinity was about 60 % for both samples. These data indicate that the addition of nanoparticles has little impact on the nanostructure, as qualitatively confirmed by SEM (**Figure 12**).

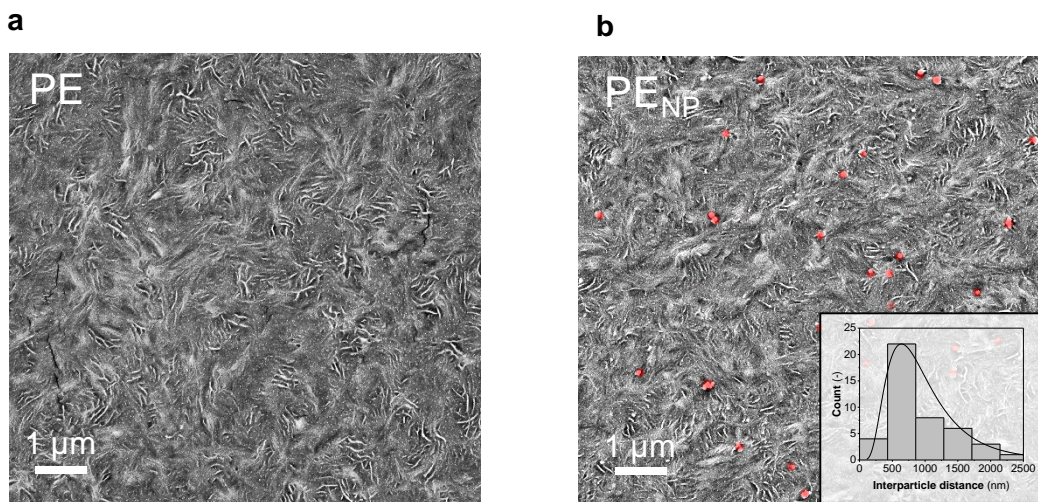


**Figure 12**, SEM image of reference LDPE, PE (a) and LDPE with 3 wt% Al<sub>2</sub>O<sub>3</sub>, PE<sub>NP</sub> (b). Nanoparticles are highlighted in red.

The DC-conductivity was measured at an electric field of 31 kV mm<sup>-1</sup> and 60 °C by following the charging current as a function of time. The behaviour of the charging current can be described by using a power law dependence:

$$i(t) \propto t^{-n} \quad (10)$$

where  $i(t)$  is the charging current over time,  $t$ . The power factor  $n$  is the absolute value of the slope in a log-log plot of the charging current. The value of  $n$  is indicative of the dominating type of transport mechanism<sup>128</sup>. The curve for neat PE shows a decline with  $n \sim 0.4$  (**Figure 13a**), which is typical for a DC-current that is governed by a build-up of space charge and trapping<sup>70</sup>. For PE<sub>NP</sub> a different behaviour is observed with a maximum of  $n \sim 2$  at  $t \sim 30$  s. After  $t \sim 4000$  s the charging current declines more slowly and approaches a constant value. The dramatic initial decrease in charging current could be the result of a slow polarisation process as suggested by Hoang et al<sup>70</sup>. The final DC-conductivity ( $\sigma$ ) extracted after 11 h was for PE  $\sigma \sim 1.5 \cdot 10^{-14}$  S m<sup>-1</sup> and for PE<sub>NP</sub>  $\sigma \sim 1.4 \cdot 10^{-15}$  S m<sup>-1</sup>, which is a decrease by one order of magnitude. The decline in conductivity may be the result of a reduced charge carrier mobility due to the presence of charge traps at the interface of the nanoparticles, which several authors have suggested previously<sup>68, 88, 129</sup>.

Electrical treeing is a commonly used phenomenon for evaluating the dielectric strength of an AC insulation material. The voltage that initiates the formation of an electrical tree was monitored for

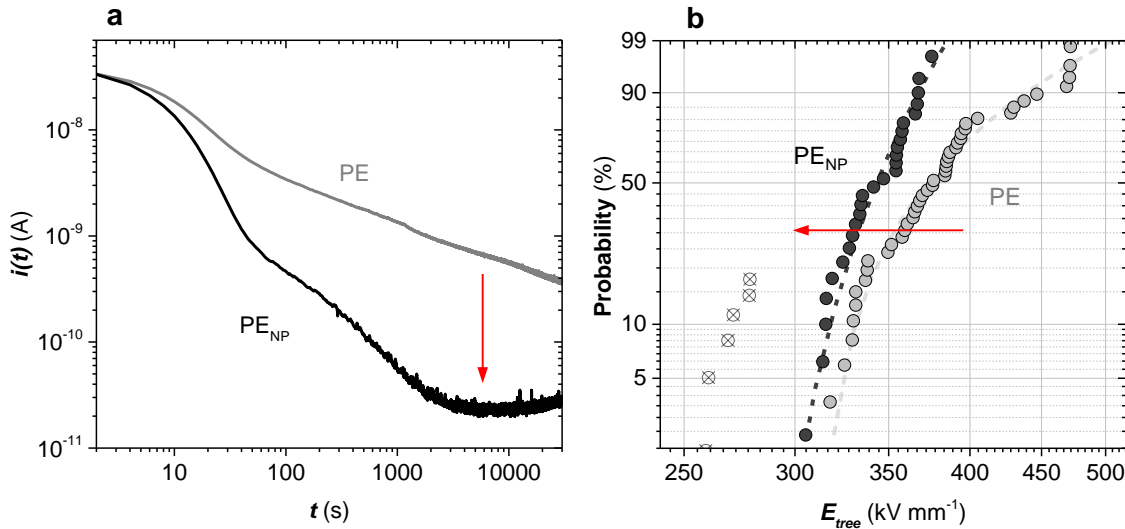


**Figure 13,** (a) Charging current of PE and PE<sub>NP</sub> measured at 60°C and 31 kV mm<sup>-1</sup>. (b) 3-parameter Weibull distribution plot of PE and PE<sub>NP</sub>.

a number of samples of both neat PE and PE<sub>NP</sub> (**Figure 13b**). The electric field, at which 63% of all observed electrical trees have initiated,  $E_{63}$ , decreased by 10% from 387 kV mm<sup>-1</sup> to 350 kV mm<sup>-1</sup> for PE<sub>NP</sub> compared to PE. This decrease in breakdown strength was also observed by Wang et al <sup>69</sup>.

It is feasible that the nanoparticles introduce defects, such as voids due to a poor interaction with the polyethylene matrix, which would lead to local field enhancement. Chen et al have shown that a thermally aged nanocomposite performed better than unaged samples <sup>130</sup>. It was proposed that the thermal treatment at 60 °C could lead to a diffusion of PE to the interface of the particles filling the voids around particles. It should be noted that the thermal treatment made in Cheng's paper also affected the nanostructure of PE. Evidently, the addition of Al<sub>2</sub>O<sub>3</sub> nanoparticles results in a lower DC-conductivity but also lower AC breakdown strength, which implies a trade-off between AC and DC properties.

### 8.1 Functionalisation of nanoparticles with a thioxanthone voltage stabiliser

In an attempt to counter the decrease in breakdown strength of the nanocomposite a voltage stabiliser was added. Voltage stabilisers have been used to improve the breakdown strength of polyethylene. For instance Jarvid et al have shown that stabilisers can increase the breakdown strength by up to 148% <sup>38</sup>. In this thesis a thioxanthone-based stabiliser was attached to the surface of the particles (PE<sub>NP-VS</sub>) (**Figure 14**). The thioxanthone core was found to increase the breakdown strength of LDPE when functionalised with a variety of different pendant groups <sup>34</sup>. In this study a thioxanthone core was functionalised with a carboxylic acid in order to promote attachment to the Al<sub>2</sub>O<sub>3</sub> nanoparticle surface. The voltage stabiliser was also mixed with nanoparticles without attachment (PE<sub>NP:VS</sub>). As a control the pure voltage stabiliser in LDPE was also tested (PE<sub>VS</sub>).

The functionalisation of the nanoparticles was analysed using TGA and FT-IR. TGA shows a weight decrease of about 1%, which arises from degradation of the stabiliser on the nanoparticle surface (**Figure 15b**). FT-IR confirms functionalisation of thioxanthone by revealing additional signals at 1628 and 1438-1216 cm<sup>-1</sup>, which can be assigned to carbonyl and aromatic carbon-carbon bonds respectively found in the voltage stabiliser (**Figure 15c**). TEM images of the functionalised

nanoparticles reveal a 4.5 nm thin halo on the particle surface, which corroborates binding of the voltage stabiliser (**Figure 15a**).

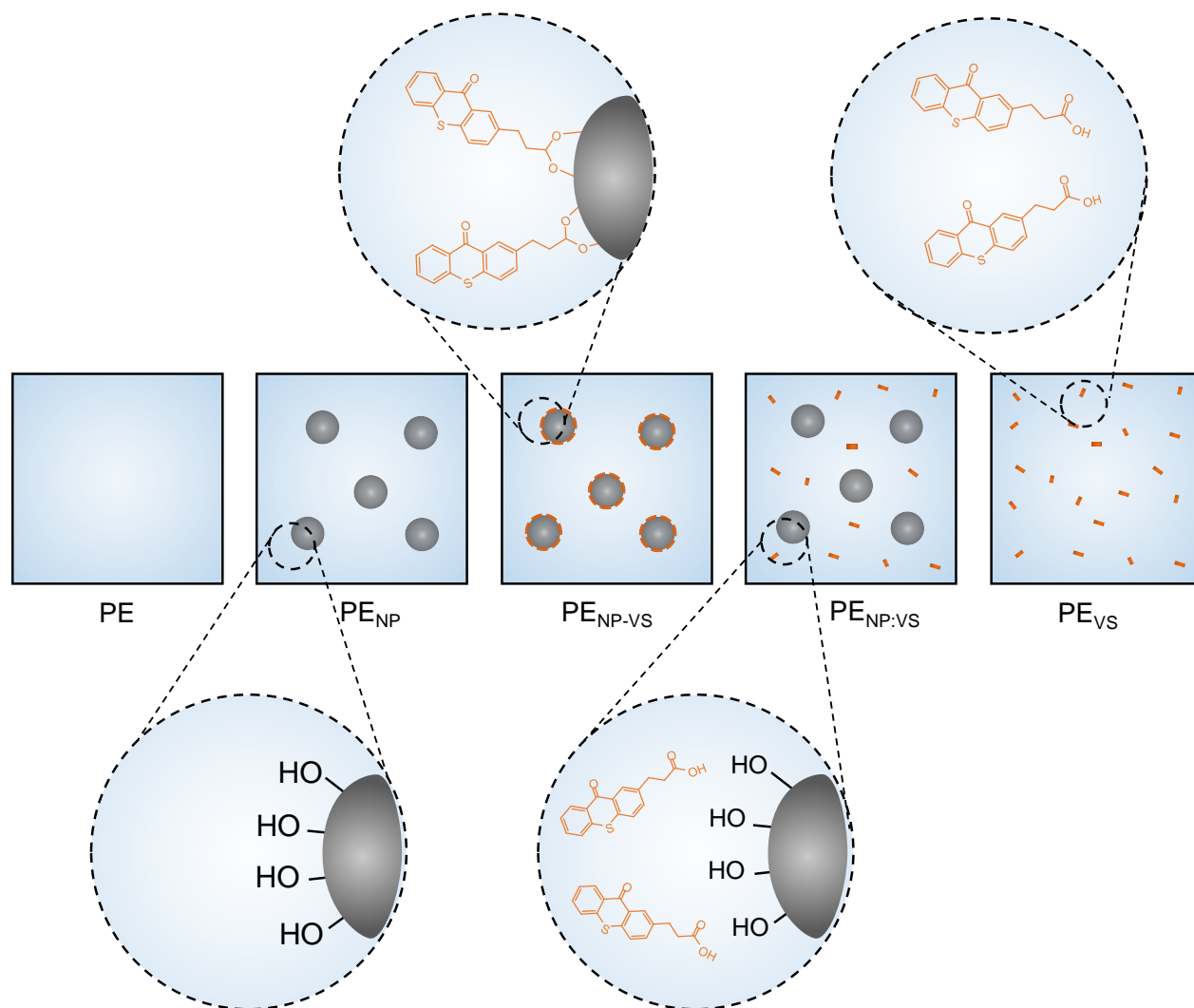


**Figure 14**, Schematic illustration of nano composite samples. PE is the reference LDPE, PE<sub>NP</sub> contains 3 wt% Al<sub>2</sub>O<sub>3</sub>, PE<sub>NP-VS</sub> contains 3 wt% functionalised Al<sub>2</sub>O<sub>3</sub>, PE<sub>NP:VS</sub> contains 3 wt% Al<sub>2</sub>O<sub>3</sub> and 0.03 wt% stabiliser and PE<sub>VS</sub> contains 0.03 wt% stabiliser.

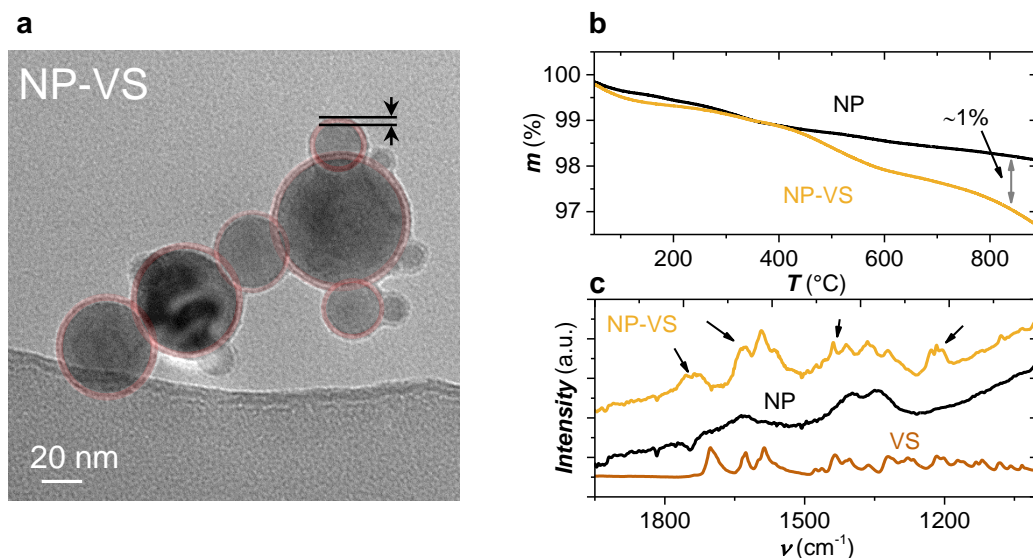


**Figure 15,** (a) TEM image of functionalised Al<sub>2</sub>O<sub>3</sub>, thioxanthone halos are highlighted in red. (b) TGA trace of functionalised Al<sub>2</sub>O<sub>3</sub> (NP-VS) and non-functionalised Al<sub>2</sub>O<sub>3</sub> (NP) (c) FT-IR of NP-VS, NP and pure voltage stabiliser.

To investigate the impact of the thioxanthone voltage stabiliser on the electrical properties of Al<sub>2</sub>O<sub>3</sub> nanocomposite DC-conductivity and electrical treeing experiments were performed. The DC charging current recorded for both the sample with stabiliser-functionalised nanoparticles (PE<sub>NP-VS</sub>), and the sample with none-attached voltage stabiliser (PE<sub>NP:VS</sub>) displays the same initial drop as observed for PE<sub>NP</sub> with a slope of  $n \sim 2$  (**Figure 16a**). However, at  $t \sim 100$  s the behaviour of both PE<sub>NP:VS</sub> and PE<sub>NP-VS</sub> differs from PE<sub>NP</sub>. Instead of a further decay in charging current the current starts to level off and hence features a conductivity comparable to that of neat PE. It appears that addition of the voltage stabiliser to the surface deprives the nanoparticle of its ability to trap charges.

Treeing data for stabiliser-functionalised nanoparticles (PE<sub>NP-VS</sub>) reveal a further decrease in breakdown strength ( $E_{63}$ ) of  $\sim 10\%$  from 338 to 312 kV mm<sup>-1</sup> for PE<sub>NP-VS</sub> compared to PE<sub>NP</sub> (**Figure 16b**). Instead, for PE<sub>NP:VS</sub> the breakdown strength recovered to  $E_{63} \sim 396$  kV mm<sup>-1</sup>, which is a value just above that measured for neat PE (387 kV mm<sup>-1</sup>).

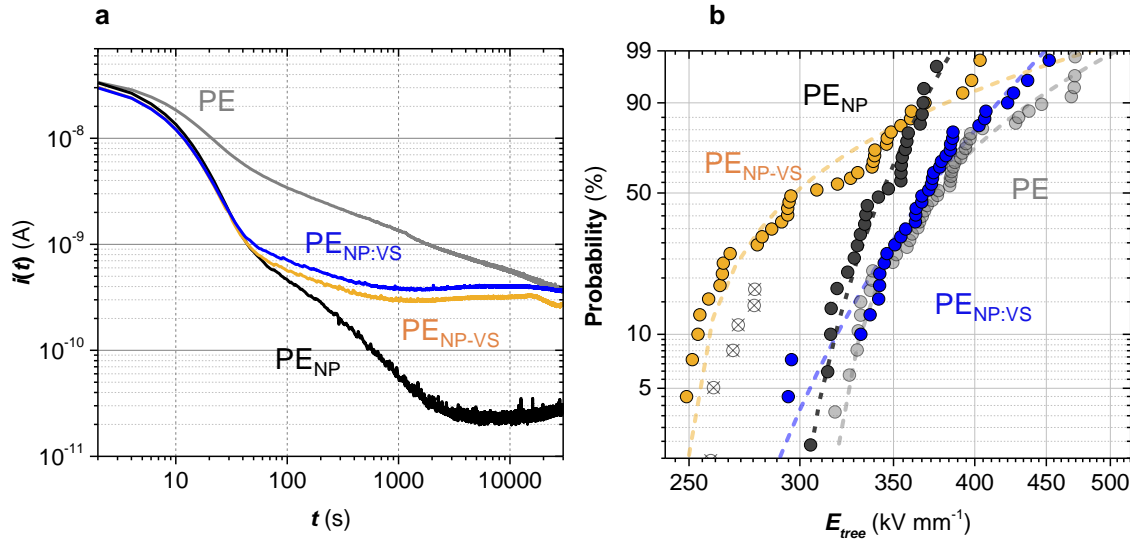


**Figure 16, (a)** Charging current recorded for PE, PE<sub>NP</sub>, PE<sub>NP:VS</sub> and PE<sub>NP:VS</sub> at 60°C and 31 kV mm<sup>-1</sup>. **(b)** 3-parameter Weibull distribution plot of PE, PE<sub>NP</sub>, PE<sub>NP:VS</sub> and PE<sub>NP:VS</sub>.

Jarvid et al. argued that a voltage stabiliser must be able to diffuse in the insulation material<sup>33</sup>, which allows the additive to accumulate at weak points in the polyethylene where electrical tree initiation is most likely to occur. A similar mechanism would explain why the attached thioxanthone has little influence on the AC treeing behaviour (PE<sub>NP:VS</sub>), whereas simple addition of the voltage stabiliser increases the AC breakdown strength (PE<sub>NP:VS</sub>).

The results of this study indicate that metal oxide nanocomposites feature a lower DC-conductivity but can suffer from a lower AC breakdown strength. The decrease in breakdown strength could be countered with a voltage stabiliser. However, the addition of a voltage stabiliser compromises the decrease in DC-conductivity. The decrease in DC-conductivity upon the addition of metal oxide nanoparticles may result from charge trapping at the nanoparticle-polyethylene interface. Conversely, the same interface may lead to a reduction in AC breakdown strength. It is generally recognised by the research community that many of the electrical effects of nanocomposites occur at the interface between particle and matrix<sup>84, 87, 88</sup>. If the effects are merely due to the properties of the surface, any kind of nano-filler with the same surface properties would have a comparable effect. If this was the case, particles with a surface that is more compatible with the polyethylene matrix could be used. Such nanoparticles could consist of polymers, which are more likely to create a more compatible interface and would also be more inviting for cable manufacturers as aggregates may be less harmful than metal oxide clusters. Another alternative route towards a large interface

area is the use of polymer blends, which can be structured on the nanoscale. In the following chapters blends of HDPE and LDPE will be explored as an alternative way of improving the electrical but also mechanical properties of LDPE.



# 9

## LDPE/HDPE blends

In this chapter the work on blends of LPDE and HDPE is discussed. A wide range of compositions are considered for both thermoplastic and crosslinked materials. First, the nanostructure of the here investigated polyethylene blends is discussed in detail, followed by DC-conductivity and AC electrical breakdown measurements. Finally, the mechanical properties of thermoplastic blends are explored.

### 9.1 Co-crystallisation

The solidification behaviour of the investigated LDPE/HDPE blend system was studied with thermal analysis. The amount of HDPE added to LDPE (in wt%) is denoted  $f_{HDPE}$ . Second heating

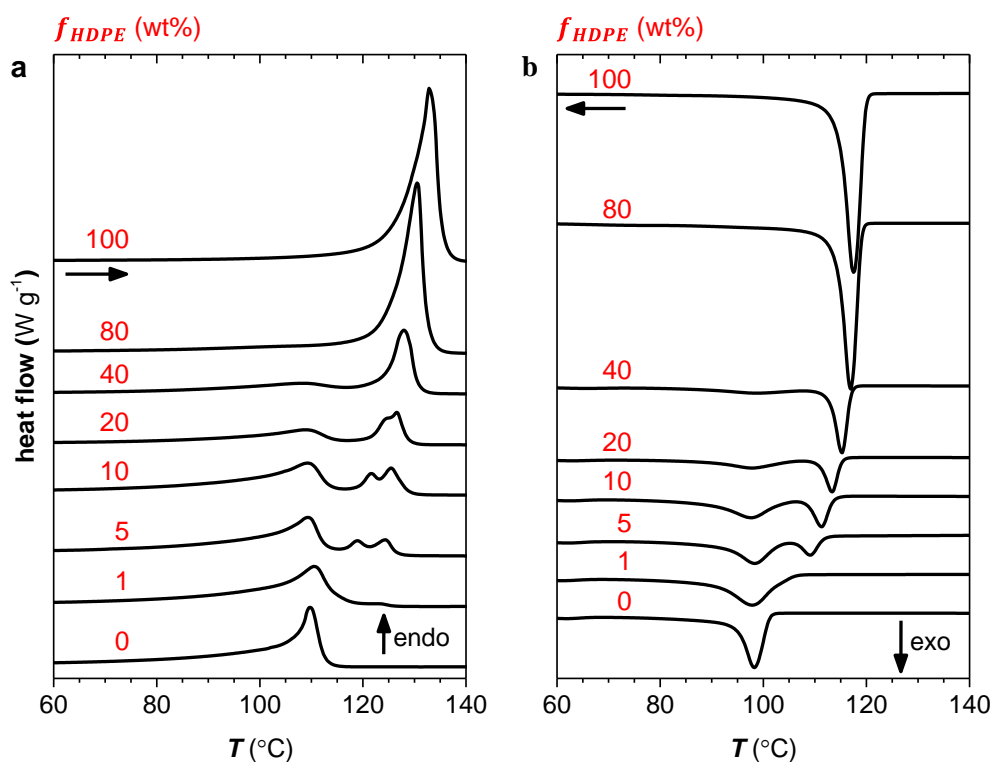


**Figure 17**, DSC second heating (a) and cooling (b) thermograms of LDPE/HDPE blends recorded between  $-20$  and  $160$   $^{\circ}\text{C}$  at a rate of  $\pm 10$   $^{\circ}\text{C min}^{-1}$ .

DSC thermograms of blends with  $f_{HDPE} \leq 40$  wt% feature a melting peak at  $T_m^{LDPE} \sim 110$  °C for LDPE, which remains at the same position (**Figure 17**). Instead, for neat HDPE a melting peak is observed at  $T_m^{HDPE} \sim 133$  °C, which shifts to lower temperatures with increasing amount of LDPE. This melting point depression arises because the HDPE fraction dissolves in already molten LDPE before reaching the melting temperature of neat HDPE. For blends containing  $f_{HDPE} = 5$  wt% to 20 wt% a third melting peak is observed at intermediate temperatures between  $T_m^{LDPE}$  and  $T_m^{HDPE}$ . This peak can be attributed to co-crystallisation of sufficiently long linear LDPE segments and HDPE chains. The tendency for co-crystallisation strongly depends on the cooling rate. Rapid cooling promotes the formation of co-crystals (**Figure 18**). Instead, slow cooling at a rate of  $-1$  °C  $\text{min}^{-1}$  avoids co-crystallisation. The here described co-crystallisation behaviour has been reported by a number of previous studies, as discussed in more detail in Chapter 6.

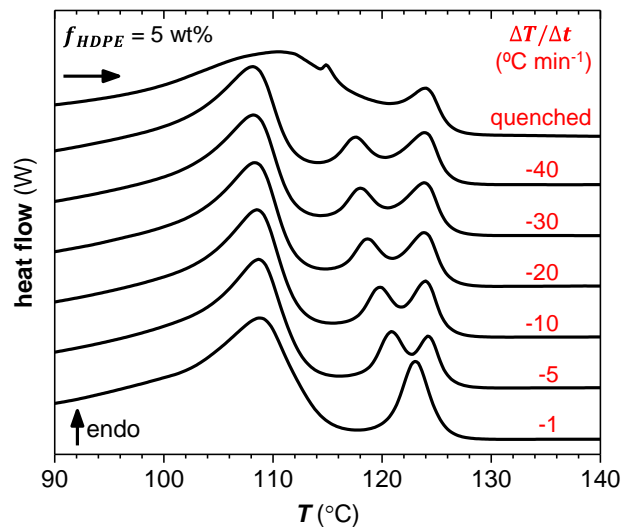


**Figure 18**, DSC second heating scans of a blend with 5 wt% HDPE after cooling from the melt at 150 °C with rates ranging from  $\Delta T/\Delta t = -1$  to  $-40$  °C  $\text{min}^{-1}$ .

Neat HDPE has a crystallinity of  $X_{HDPE} \sim 81\%$  compared to LDPE with  $X_{LDPE} \sim 55\%$ . Blends feature an intermediate crystallinity. To compare the crystallinity of HDPE and LDPE-rich crystals the melting endotherms were separated into a LDPE and HDPE part, where the HDPE part included the co-crystals. As expected,  $X_{LDPE}$  decreases, whereas  $X_{HDPE}$  increases linearly.

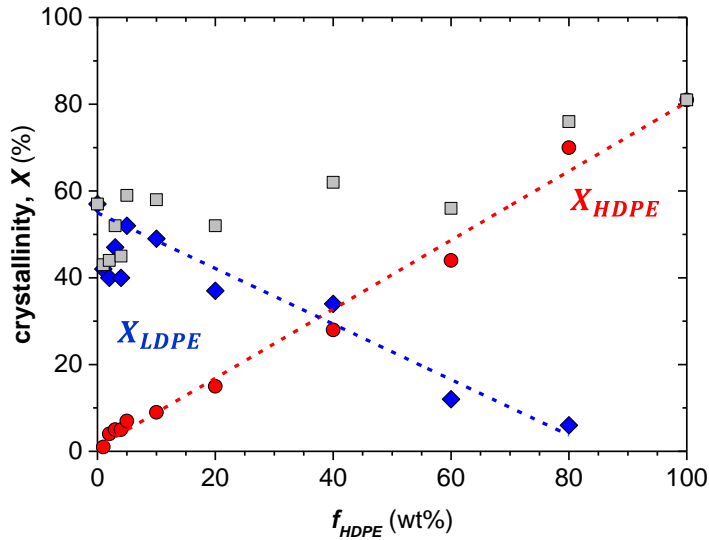


**Figure 19**, Crystallinity of the LDPE ( $\blacklozenge$ ) and HDPE fraction ( $\bullet$ ), as well as the total crystallinity ( $\blacksquare$ ) as a function of HDPE fraction. For  $X_{LDPE}$  deviation from a linear trend occurs for  $f_{HDPE} \leq 4\%$  because the LDPE and HDPE peak are difficult to separate.

## 9.2 Phase diagram

A temperature-composition diagram was constructed by using the melting peaks obtained from thermal analysis (**Figure 20**). Four zones can be identified. At high temperatures a homogenous melt exists, denoted  $L$ . As the temperature is decreased below  $T_m^{HDPE}$  a region is encountered where HDPE crystals are surrounded by a LDPE-rich melt ( $L + S_{HDPE}$ ). For blends with  $f_{HDPE} \leq 20$  wt% co-crystals are also present ( $+S_{CO}$ ). At temperatures below  $T_m^{LDPE} \sim 110$  °C both HDPE and LDPE are solid ( $S_{LDPE} + S_{HDPE}$ ). Besides HDPE and LDPE crystals there are co-crystals for  $f_{HDPE} \leq 20$  wt%. In addition to polyethylene crystals a certain amount of amorphous material remains present.

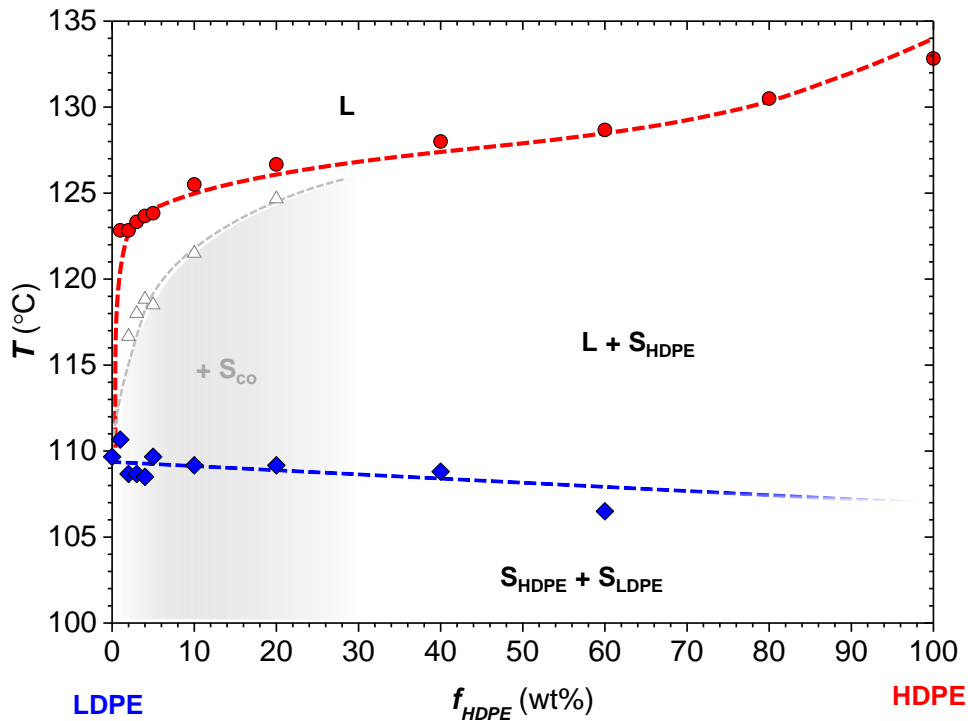


**Figure 20**, LDPE/HDPE temperature-composition diagram constructed using peak melting temperatures of LDPE ( $\blacklozenge$ ), HDPE ( $\bullet$ ) and co-crystals ( $\triangle$ ).

### 9.3 Diffusion of HDPE into LDPE confirms miscibility

The miscibility of HDPE and LDPE was confirmed with a cross-polarised optical microscope equipped with a heat stage. Films of neat LDPE and HDPE with a thickness of 0.1 mm were placed next to each other. Annealing for 90 min at 145 °C allowed HDPE to diffuse across the common interface into LDPE, and *vice versa*. The diffusion of HDPE into LDPE can be visualised by examining at which temperature different parts of the sample start to crystallise during cooling from the melt. Close to the HDPE/LDPE interface and in the film that initially consisted of neat LDPE, crystallisation commences above  $T_c^{LDPE}$  (**Figure 21**). This observation confirms diffusion and hence miscibility of LDPE and HDPE in the melt.

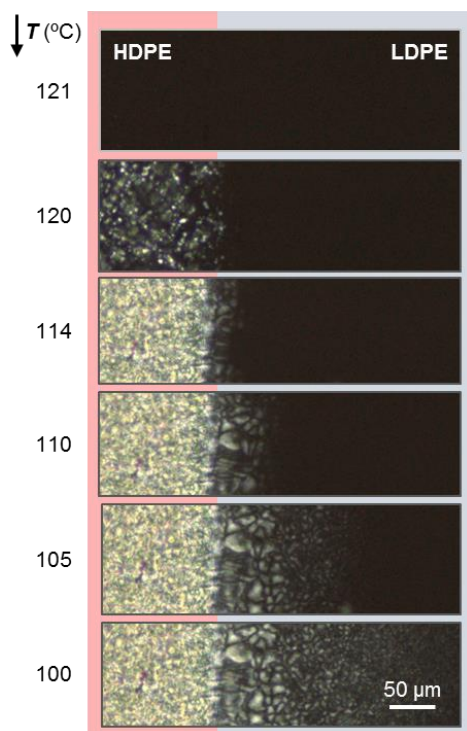


**Figure 21**, Cross-polarised optical micrographs of 0.1 mm thick adjacent films of neat HDPE and LDPE recorded during cooling at  $10\text{ °C min}^{-1}$  after annealing the melt at 145 °C for 90 min, allowing the two polyethylenes to diffuse across the joint film boundary.

## 9.4 Distribution of crystal lamellae

Thermal analysis and optical microscopy suggest that there is miscibility of HDPE and LDPE in the melt. Phase separation occurs through crystallisation where the two components form crystals of different thicknesses. SAXS was carried out in order to study the distribution of crystal lamellae in more detail.

Kratky plots ( $q^2I$  vs  $q$ ), of the recorded SAXS data reveal a single broad (first order) scattering peak of LDPE at  $q_{p,LDPE} = 0.47 \text{ nm}^{-1}$ . For HDPE a first order peak is found at  $q_{p,HDPE} = 0.26 \text{ nm}^{-1}$  followed by the second order peak at  $0.53 \text{ nm}^{-1}$ . The second order peak in case of HDPE is the result of a more coherent repetition of the lattice planes compared to LDPE, for which only one peak can be resolved. For blends with  $f_{HDPE} \leq 20 \text{ wt\%}$  only a *single* scattering peak is observed suggesting that HDPE and LDPE lamellae form random stacks (**Figure 22**). Instead, for a phase-separated system *two* scattering peaks would be expected because HDPE and LDPE crystallised in distinct domains, forming two types of lamellar stacks. To illustrate a diffractogram of a phase-separated system, a sample consisting of a sandwich of a neat HDPE and a neat LDPE film was measured (**Figure 22**). Evidently, the SAXS diffractogram of such a clearly phase-separated system is a superposition of the SAXS patterns of neat HDPE and LDPE, which results in *two*

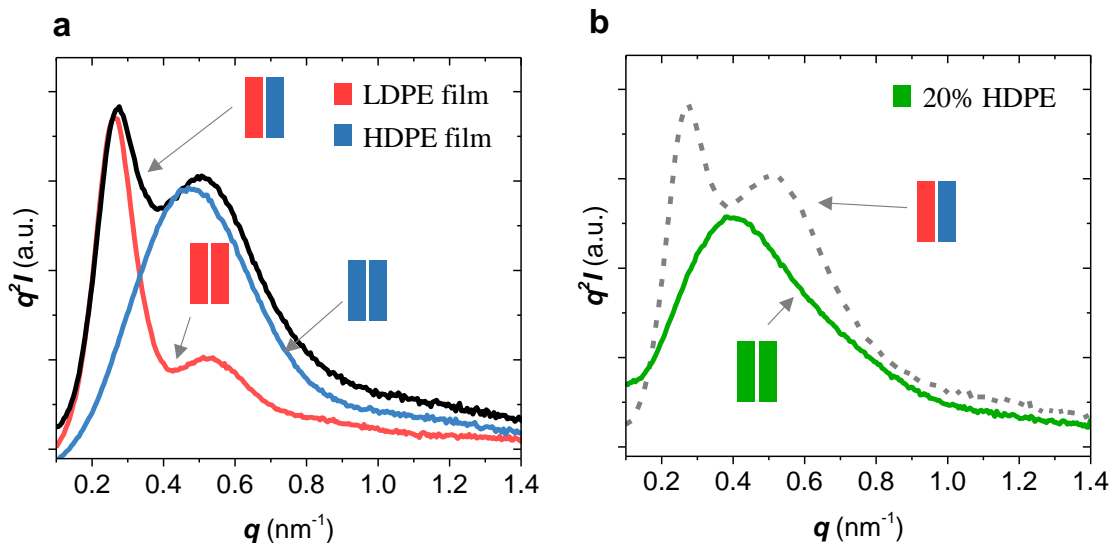


**Figure 22,** (a) Kratky plots of SAXS data recorded for HDPE (red), LDPE (blue) and a sandwich of a HDPE and LDPE film (red/blue). Two distinct peaks are observed in the mixed sample, which is characteristic for a phase-separated system. (b) SAXS data for 20 wt% HDPE (green) showing a single peak. Dashed line is the HDPE-LDPE sandwich.

clearly discernible peaks. The fact that the studied LDPE/HDPE blends only give rise to a single scattering peak is consistent with crystallisation from a homogeneous melt, leading to a random stack of HDPE and LDPE lamellae, as well as co-crystals.

From SAXS the long period can be extracted by  $L_p = 2\pi/q_p$ . For a one-dimensional stack of crystalline lamellae that are separated by layers of amorphous material  $L_p$  corresponds to the combined thickness of these layers (cf. Chapter 4). Hence  $L_p$  scales with the average distance between lamellae. The lamellar thickness can be calculated by considering the crystallinity, as  $l_{SAXS} = X \cdot L_p$  (cf. Chapter 4). The lamellar thickness of LDPE and HDPE was 6.9 nm and 18.6 nm, respectively, in agreement with values calculated from DSC melting peaks (7.7 nm and 21.5 nm). The lamellar thickness calculated from SAXS increases linearly with  $f_{HDPE}$ .

Variable-temperature SAXS was used to monitor the evolution of the long period upon heating. For LDPE  $q_p$  continuously shifts to lower values upon heating from ambient to 125 °C (**Figure 23**). Thin crystals gradually melt even far below  $T_m^{HDPE} \sim 110$  °C, which results in a continuous increase in the average distance between the remaining crystalline lamellae. Above  $T_m^{LDPE}$  the scattering signal disappears. For HDPE  $q_p$  does not change until the temperature reaches  $\sim 120$  °C, above which  $q_p$  decreases until complete melting occurs around  $T_m^{HDPE} \sim 133$  °C. The blend of  $f_{HDPE} = 5$  wt% shows a similar behaviour as LDPE up to  $T_m^{LDPE}$ . However, for the temperature interval  $T_m^{LDPE} < T < T_m^{HDPE} \sim 124$  °C a weak scattering signal remains present, corresponding to  $L_p \sim 57$  nm at 115 °C (cf. Paper IV). The use of  $l_{SAXS} = X \cdot L_p$  yields an unfeasibly low value for the lamellar thickness (0.7 nm), which implies that the remaining lamellae are not arranged in one-dimensional stacks. For  $f_{HDPE} = 40$  wt% the scattering vector remains constant until about 80 °C, which is consistent with the more HDPE-like character at this stoichiometry. At higher temperatures  $q_p$  gradually decreases until  $T_m^{HDPE} \sim 128$  °C is reached, above which the scattering signal disappears.

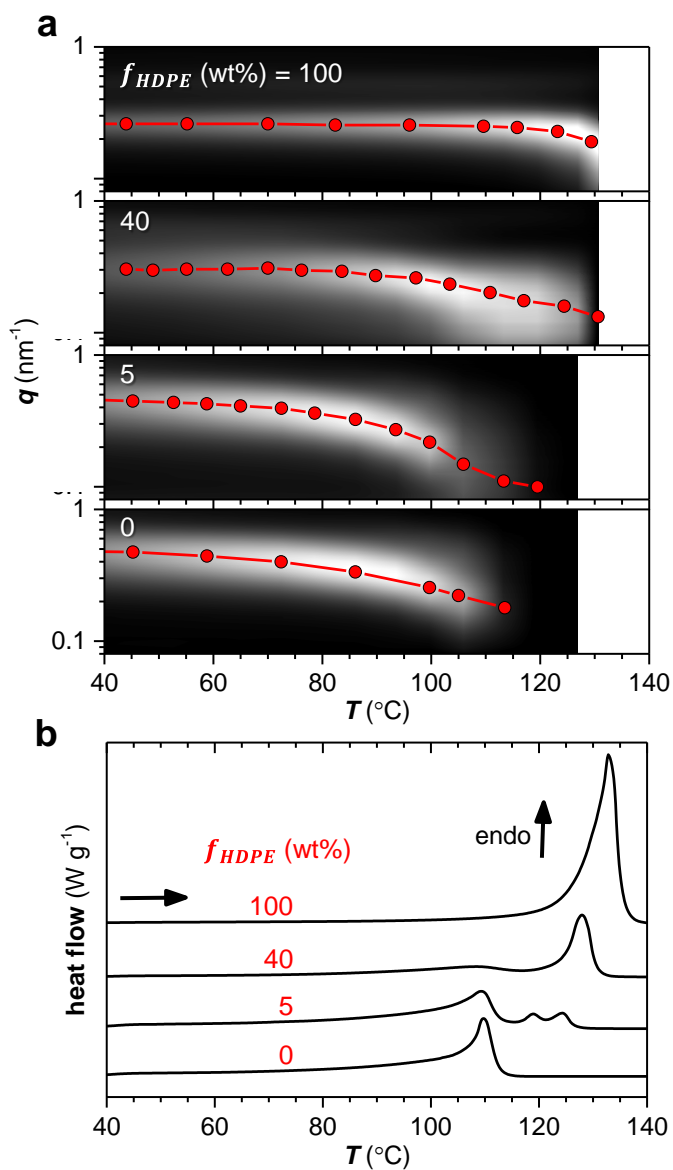


**Figure 23,** (a) Contour maps summarising Kratky plots of SAXS patterns for neat LDPE and HDPE as well as blends with  $f_{HDPE} = 5$  and 40 wt%, recorded during heating from 35 to 130  $^{\circ}\text{C}$  at a rate of 10  $^{\circ}\text{C min}^{-1}$ . (b) Corresponding DSC second heating thermograms.

### 9.5 Impact of HDPE on blend nanostructure

The nanostructure of the blends was visualised with SEM. Cryo-fractured surfaces were imaged after etching and sputtering with gold (**Figure 24**). LDPE features a fine-grained crystalline texture. The addition of 1 wt% HDPE leads to a noticeable change in the nanostructure, as evidenced by the emergence of more well-defined lamellae. For  $f_{HDPE} \sim 5$  wt% a population of thicker lamellae is present. SEM images confirm that the addition of only small amounts of HDPE is sufficient to strongly impact the nanostructure of the material.

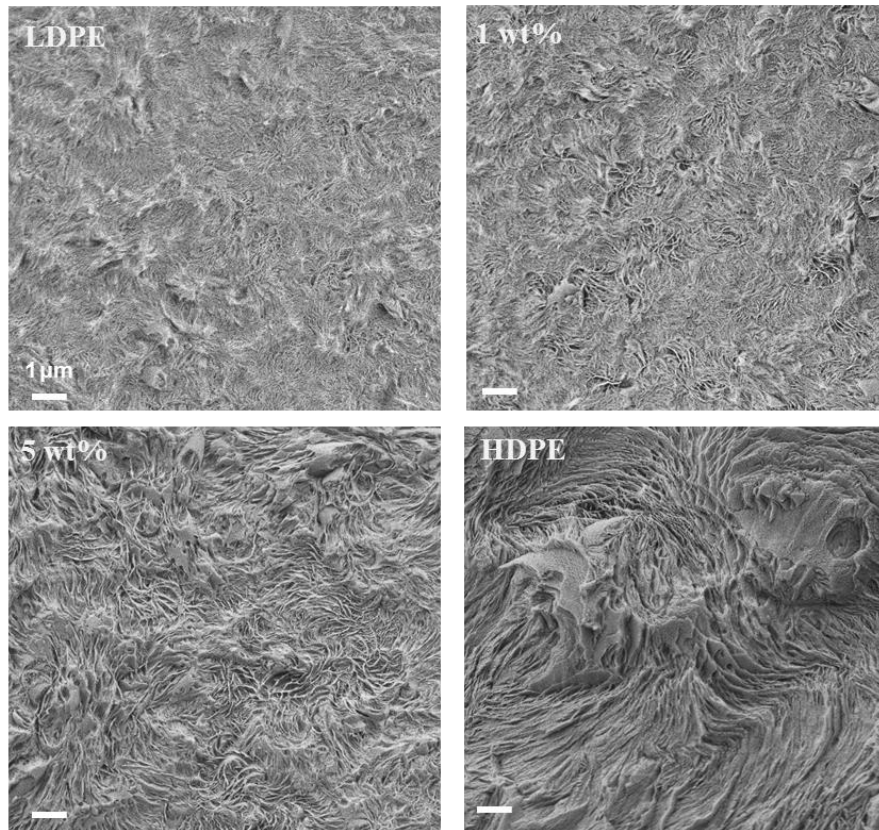


**Figure 24**, SEM images of cryo-fractured and etched surfaces corresponding to neat LDPE and HDPE as well as blends with  $f_{HDPE} = 1$  and 5 wt%.

## 9.6 DC-conductivity of LDPE/HDPE blends

In this chapter the DC-conductivity of the polyethylene blends is discussed. The strong interplay between the nanostructure and electrical properties of polyethylene (cf. Chapter 4) promises that even small amounts of HDPE significantly alter the DC-conductivity of LDPE. The blend compositions used for the conductivity measurements are displayed in **Table 1**. Crosslinked blends are denoted XLPE- and thermoplastic blends LDPE-. The DC-conductivity was measured on 1 mm thick films that were melt-pressed first at 130 °C and then 180 °C. Crosslinking occurred during the second step provided that the samples contained DCP (see Paper II for details).

*Table 1, Field strength (E-field) and temperature (T) for tested blends*

| Sample                   | $f_{\text{HDPE}}$ (%)             | E-field<br>(kV mm <sup>-1</sup> ) | T (°C) |
|--------------------------|-----------------------------------|-----------------------------------|--------|
| Thermoplastic<br>(LDPE-) | 0, 5, 10, 100                     | 30                                | 70     |
| Cross-linked<br>(XLPE-)  | 0, 1, 2, 3, 5, 10,<br>20, 40, 100 | 30, 40                            | 70,90  |

### 9.6.1 Thermoplastic blends

The DC-electrical behaviour was monitored at 30 kV mm<sup>-1</sup> and 70 °C for 24 h. The shape of the recorded charging current differs considerably between LDPE and HDPE. LDPE displays a slow decrease in charging current with an absolute slope of  $n < 1$  after 10 s (cf., eq 10). Instead, HDPE gives rise to a dramatic decrease with  $n \sim 5$  between 10 and 100s (**Figure 25**). The charging current after 100s is rather noisy, which most likely is a result of the measurement approaching the sensitivity limit of the instrument. As discussed in Chapter 8 the slope is associated with the dominating type of charge transport mechanism<sup>131</sup>. In the case of LDPE the absolute slope is  $n < 1$ , which suggests that the transport is most likely dominated by the formation of space charges<sup>132, 133</sup>. The considerable decrease of the charging current at early times is similar to the behaviour observed for Al<sub>2</sub>O<sub>3</sub> nanocomposites (cf. Chapter 8; **Figure 13**). Hoang et al<sup>70</sup> found for Al<sub>2</sub>O<sub>3</sub> nanocomposites that such a dramatic decrease can originate from slow polarisation. Evidently, the introduction of a small population of thicker crystals is sufficient to introduce charge traps that cause a significant decrease in charging current. The conductivity was calculated from the charging

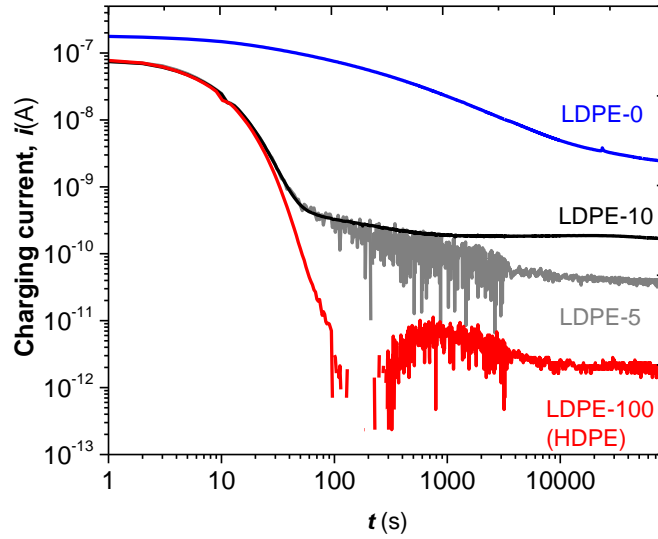


**Figure 25**, Charging current  $i(t)$  for thermoplastic blends at an electric field of  $E = 30 \text{ kV mm}^{-1}$  and  $70 \text{ }^\circ\text{C}$ .

current measured after 24h. For neat LDPE and HDPE a value of  $\sigma \sim 10 \cdot 10^{-15} \text{ S m}^{-1}$  and  $\sigma \sim 0.1 \cdot 10^{-15} \text{ S m}^{-1}$  was obtained (**Figure 27**). For blends with  $f_{HDPE} \sim 5$  and 10 wt% the DC-conductivity was almost one order of magnitude lower than that of neat LDPE, adopting a value of  $0.2 \cdot 10^{-15}$  and  $0.7 \cdot 10^{-15} \text{ S m}^{-1}$ .

### 9.6.2 Crosslinked blends

DC-conductivity measurements were also performed on a broad range of crosslinked blends. The shape of the charging current was similar to the one observed for thermoplastic blends (**Figure 26**). The DC-conductivity of the crosslinked samples extracted from  $i(t = 24h)$  was higher than the values obtained for thermoplastic blends, ranging from  $0.7 \cdot 10^{-15} \text{ S m}^{-1}$  for  $f_{HDPE} = 1 \text{ wt}\%$  to  $1.8 \cdot 10^{-15} \text{ S m}^{-1}$  for  $f_{HDPE} = 10 \text{ wt}\%$ . Neat XLPE-0 exhibited a value of  $\sigma \sim 11 \cdot 10^{-15} \text{ S m}^{-1}$  (**Figure 27**). The DC-conductivity decreased by almost one order of magnitude for  $f_{HDPE} \geq 1 \text{ wt}\%$ . It is feasible that the presence of thicker lamellae introduced charge traps that reduced the mobility of charge carriers<sup>133, 134</sup>. Since the addition of HDPE does not affect the total crystallinity for  $f_{HDPE} = 1$  to

60 wt%, the degree of ordering is unlikely to influence the electrical properties of the here studied samples.

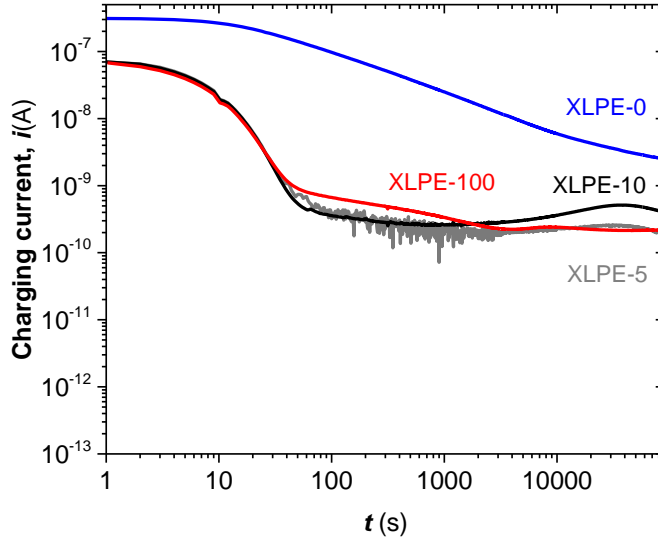


**Figure 26**, Charging current  $i(t)$  for crosslinked blends at an electric field of  $E = 30 \text{ kV mm}^{-1}$  and  $70 \text{ }^\circ\text{C}$ .

To explore the conduction mechanism further the crosslinked samples were tested at increased electric field and temperature. At a higher field of  $40 \text{ kV mm}^{-1}$  the DC-conductivity measured for neat XLPE-0 had decreased to  $8 \cdot 10^{-15} \text{ S m}^{-1}$ . Conversely, the DC-conductivity of the blends and HDPE slightly increased to approximately  $2 \cdot 10^{-15} \text{ S m}^{-1}$ . The higher conductivity may result from Poole-Frenkel conduction, which predicts a higher conduction at increased field as a result of the decrease in barrier height of the potential well of deep traps (**Figure 28**)<sup>135, 136</sup>. An increase in temperature to  $90 \text{ }^\circ\text{C}$ , while maintaining an electric field of  $30 \text{ kV mm}^{-1}$ , had a more pronounced impact on the DC-conductivity than an increase in the field. The conductivity for neat XLPE-0 and XLPE-100 increased to almost  $60 \cdot 10^{-15} \text{ S m}^{-1}$  and  $6 \cdot 10^{-15} \text{ S m}^{-1}$ , respectively. Blend samples had a conductivity in-between those values, the highest being  $\sim 20 \cdot 10^{-15} \text{ S m}^{-1}$  for XLPE-1.

LDPE/HDPE blends

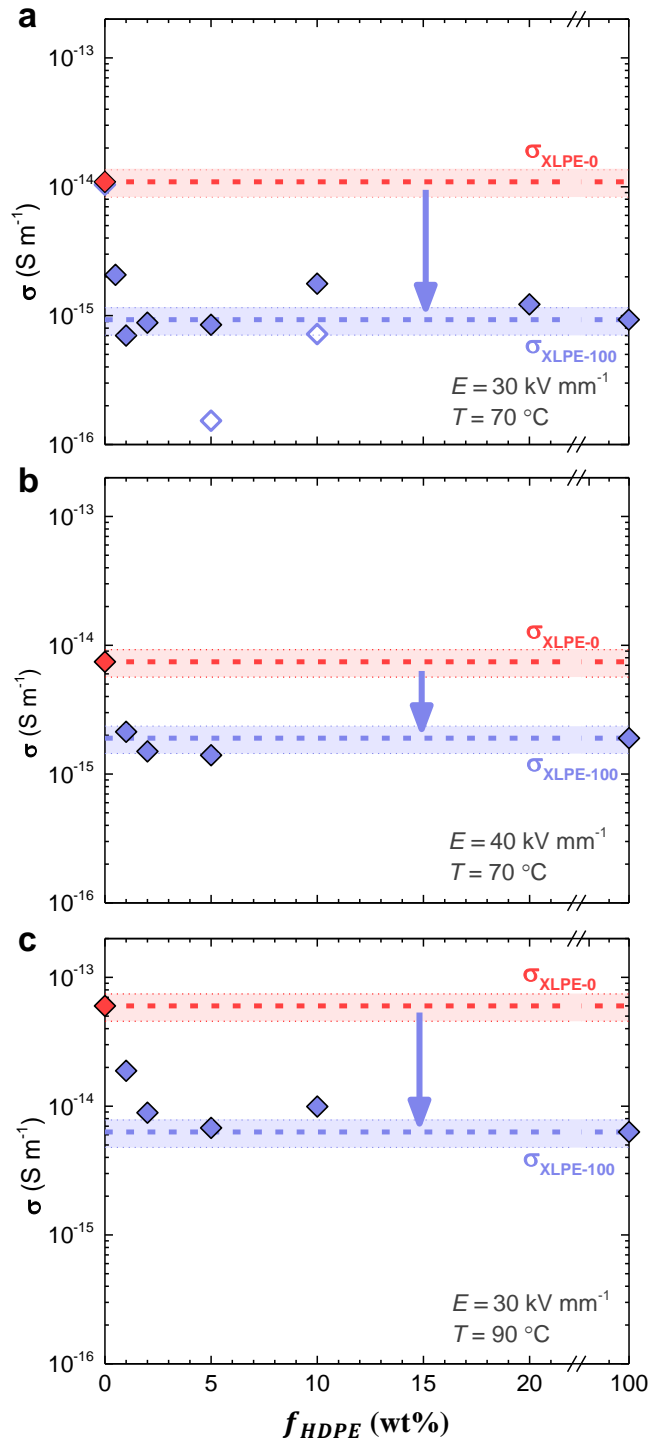


**Figure 27**, DC-conductivity after 24 h as a function of HDPE content calculated for thermoplastic (open diamonds) and crosslinked blends (filled diamonds): (a)  $E = 30 \text{ kV mm}^{-1}$  and  $T = 70 \text{ }^\circ\text{C}$  (b)  $E = 40 \text{ kV mm}^{-1}$  and (c)  $E = 40 \text{ kV mm}^{-1}$  and  $T = 90 \text{ }^\circ\text{C}$ . Dashed blue and red lines indicate the electrical conductivity of XLPE-0 and XLPE-100, respectively; the confidence interval (filled area) corresponds to a standard deviation of  $\pm 24 \%$ .

The increase in conductivity can be a result of thermally assisted hopping as well as a decrease in the amount of charge trapping crystals. The crystallinity of blends with  $f_{HDPE} \leq 10\%$  at 90 °C was ~30% compared to ~40% at 70 °C. This is a significant decrease in crystallinity that could lead to less trapping sites in the form of crystal interfaces. In summary, all measured blends (except for XLPE-1 at 90 °C) featured a lower conductivity than neat XLPE-0 both at 70 °C and 90 °C.

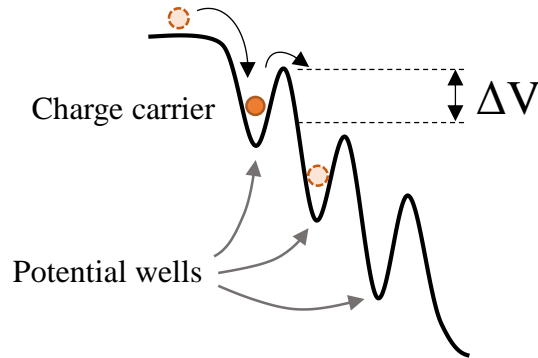


**Figure 28**, Schematic illustration of field depended Poole-Frenkel conduction.  $\Delta V$  is the potential barrier.

### 9.7 AC-breakdown of crosslinked LDPE/HDPE blends

In case of the  $Al_2O_3$  nanocomposite investigated in Chapter 8 the decrease in DC-conductivity was accompanied by a decrease in AC breakdown strength. To determine whether the blend suffer from a similar decrease in AC breakdown strength a series of electrical treeing measurements was carried out. In order to determine the AC breakdown strength with this method the sample must be transparent, since tree initiation is detected with an optical microscope. Hence, only crosslinked samples were tested in this study because of their relatively high degree of transparency. Neat HDPE was too opaque and could not be studied. The nano- and microstructure of polyethylene strongly affects the AC breakdown behaviour. For instance, Yan et al have reported that the lamellar thickness can affect the AC breakdown strength<sup>137</sup>. Since even a small amount of thicker lamellae reduced the DC-conductivity of the in this thesis studied blends (cf. Chapter 9.6), a similar influence on the AC breakdown strength was anticipated. However, all measured blends featured a similar tree inception voltage, i.e.  $E_{63} \sim 400 \text{ kV mm}^{-1}$ . The threshold value ( $E_0$ ) for XLPE-1 was somewhat lower (~17%) than for neat XLPE-0. Instead, for XLPE-5 and XLPE-10 a 20% higher value was deduced. The probability density function of treeing data recorded for both XLPE-5 and

XLPE-10 indicated a tail at higher fields, which suggests that some samples displayed an increase in AC breakdown strength. A similar trend was also described by Hosier et al who explained the increase in dielectric strength with a space filling spherulitic structure due to the presence of HDPE  
125.

## 9.8 Mechanical properties

A high-voltage cable is subjected to both electrical as well as mechanical stress during transport, installation and operation at elevated temperature. During operation the insulation heats up due to Joule heating (cf. Chapter 3), which softens the polyethylene insulation. Hence, crosslinking is necessary in order to avoid stress cracking and creep. The crosslinking step is time consuming and a degassing step is needed which also poses health issues <sup>138</sup>(Chapter 2). As discussed in Chapter 9.2, only minute amounts of HDPE are sufficient to significantly reduce the DC-electrical conductivity of an LDPE resin. In this Chapter the mechanical properties of the LDPE/HDPE blend system, which was introduced in Chapters 9.1 to 9.5, are discussed.

Tensile deformation was used to determine the Young's modulus ( $E$ ) at room temperature. Values of 180 MPa and 860 MPa were measured for neat LDPE and HDPE, respectively. For the blends the Young's modulus increased linearly with HDPE concentration. The evolution of the storage modulus ( $G'$ ) with temperature was monitored with DMA from 40 to 130 °C. At 40 °C values of  $G'_{LDPE} \sim 100$  MPa and  $G'_{HDPE} \sim 540$  MPa were measured for LDPE and HDPE, respectively (**Figure 29**). The increase in modulus could be described with the rule of mixtures (see Paper IV):

$$G' = (1 - f_{HDPE}) \cdot G'_{LDPE} + f_{HDPE} \cdot G'_{HDPE} \quad (11)$$

The modulus decreased with temperature. At 115 °C LDPE featured a value of  $G'_{LDPE} = 0.6$  MPa compared to  $G'_{LDPE-5} = 2$  MPa. Already the addition of only 1 wt% HDPE doubles the storage modulus at 115 °C to 1.5 MPa. Evidently, the presence of higher-melting HDPE crystallites reinforces the blend material above the melting temperature of LDPE. The reinforcing effect most likely originates from higher melting HDPE lamellae. Creep tests were carried out to explore whether HDPE crystallites form a continuous network. To this end, dog-bone shaped samples were suspended in an oven at 115 °C and allowed to deform under their own weight (Paper III). LDPE at 115 °C undergoes complete melting and therefore continues to elongate indefinitely. As shown in **Figure 17** even for  $f_{HDPE} \sim 1$  wt% a small population of higher-melting HDPE crystallites remain

present at 115 °C. Strikingly, as little as 2 wt% HDPE is sufficient to resist creep (**Figure 30**). This observation suggests that HDPE crystallites form a continuous, load-bearing network that allows the samples to maintain their shape even though most of the material has melted. The ability of the network to resist creep depends on the extent of co-crystallisation. Fast cooling, which promotes the formation of co-crystals (cf. Chapter 9.1), enhances creep at 115 °C. Instead, slow cooling avoids co-crystallisation and hence increases the amount of thick HDPE crystals, which leads to improved creep resistance (compare creep behaviour observed for  $f_{HDPE} \sim 1$  wt%; Figure 30). The reason for the increased creep strength is the absence of co-crystals. HDPE that has co-crystallised with LDPE leads to thinner lamellae that will melt at lower temperatures. Thus, the network of crystals that remain above the melting temperature of LDPE weakens to a greater extent at 115 °C.

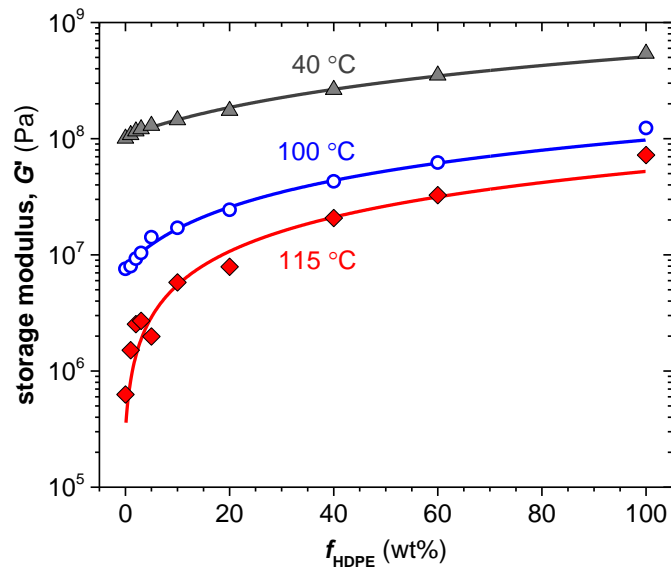


**Figure 29**, Storage modulus as a function of  $f_{HDPE}$  at 40 °C (▲), 100 °C (○) and 115 °C (◆); solid lines are fits created with a simple rule of mixtures (equation 11).

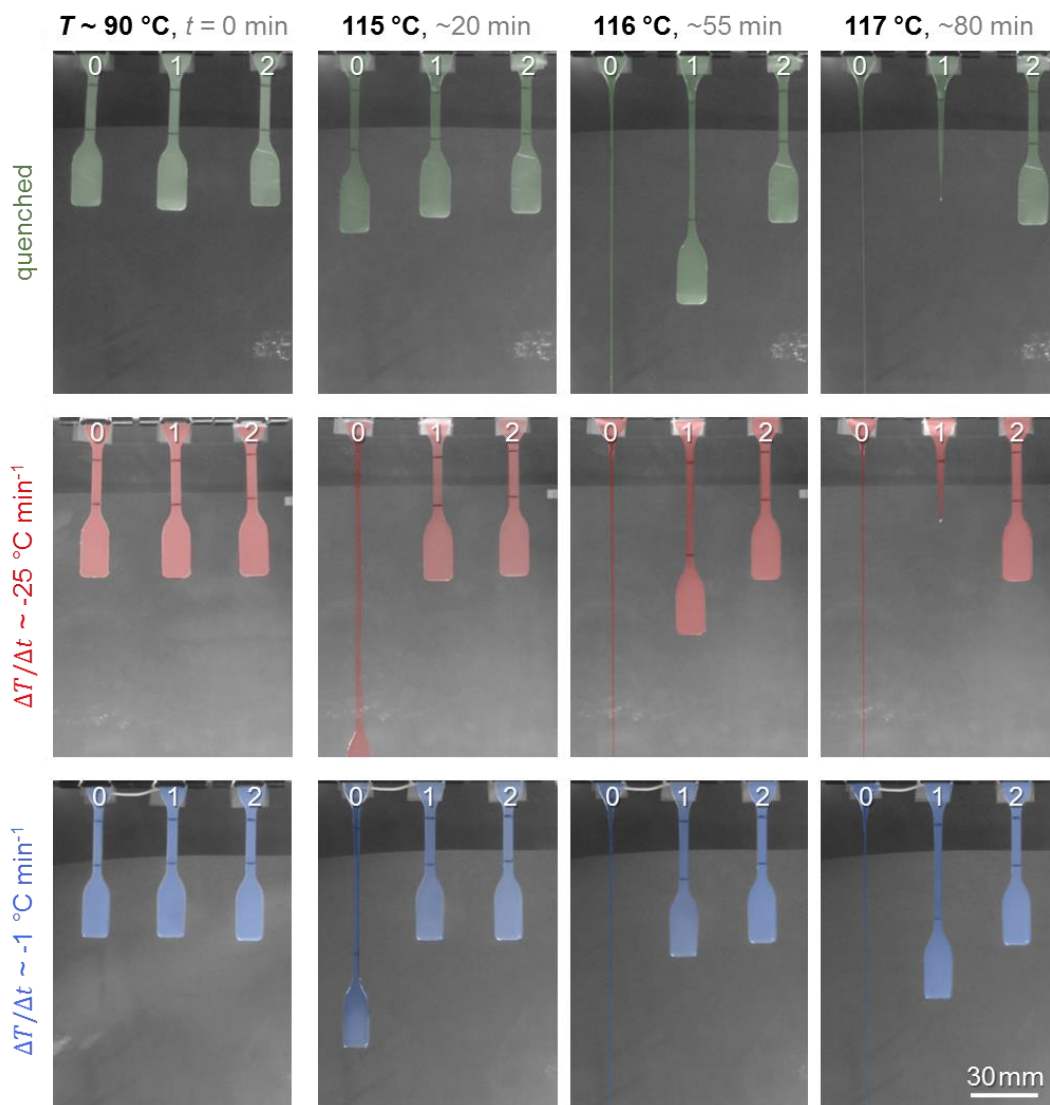


**Figure 30**, Creep elongation of neat LDPE and blends with 1 and 2 wt% HDPE under their own weight, solidified by rapid quenching (top row, green), with  $\Delta T/\Delta t \sim -25 \text{ }^\circ\text{C min}^{-1}$  (center row, red), and  $\Delta T/\Delta t \sim -1 \text{ }^\circ\text{C min}^{-1}$  (bottom row, blue). Note that samples are false-coloured to increase contrast.

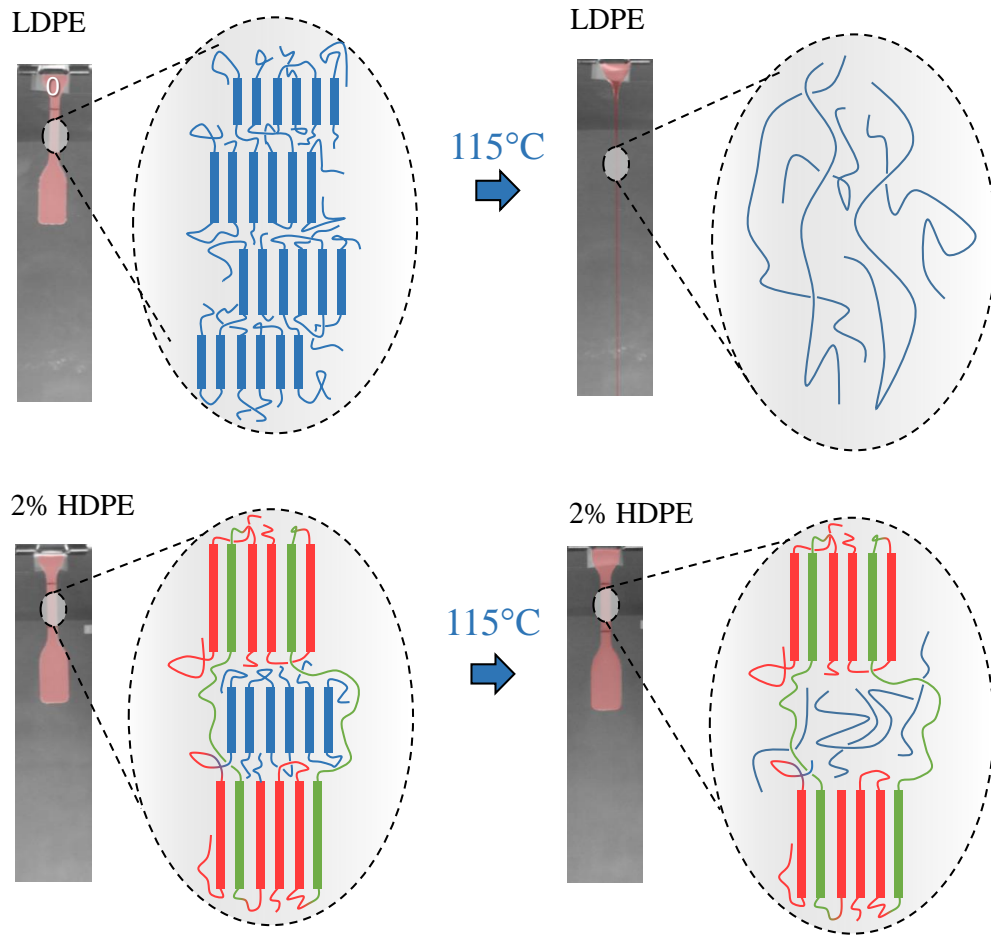


**Figure 31**, Illustration of the effect that tie chains might have in a semi-molten blend compared to molten LDPE.

The presence of a load-bearing network suggests the presence of tiechains (**Figure 31**) and/or trapped entanglements that connect the remaining HDPE crystallites above the melting temperature of LDPE. The Huang-Brown model (Chapter 4) was used to estimate the probability that a HDPE chain actually bridges the amorphous region to form a tie-chain<sup>56, 57</sup>. The probability of tie chain formation obtained from equation 6 was multiplied with  $f_{HDPE}$ .

The model assumes that “a tie chain is formed when the end-to-end distance of a molecule in the melt is equal or greater than the distance between the joining crystals, if however the end-to-end distance is shorter than the thickness of the amorphous region a tie chain will never form”<sup>57</sup>.

The upper limit of integration, which corresponds to the required end-to-end distance, was set to  $L = L_p + l_c$ , i.e. the long period measured with SAXS at 115 °C plus the lamellar thickness calculated using the Gibbs-Thomson equation for  $T_m^{HDPE}$ . This expression was used instead of

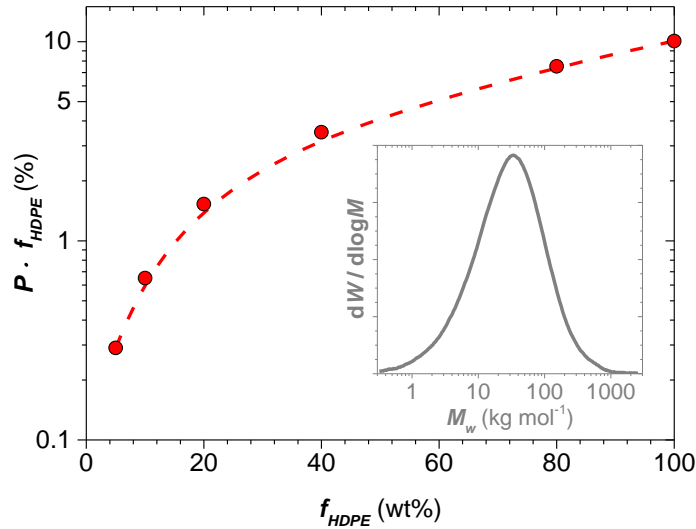


**Figure 32**, Tie chain fraction according to the Huang-Brown model at 115 °C as a function of  $f_{HDPE}$ . Inset: molecular weight distribution of HDPE.

$L = 2l_c + l_a$ , which was originally proposed by Huang and Brown.  $l_a$  could be calculated according to  $l_a = (1 - X) \cdot L_p$  provided that the remaining, higher-melting HDPE lamellae form a one-dimensional stack. However, as discussed in Chapter 9.4 this assumption leads to unphysical values for  $l_c$  (and hence  $l_a$ ). Therefore an alternative expression was used for the required end-to-end distance.

For neat HDPE the probability of tie chain formation was estimated to be 10 % at 115 °C. This probability decreases to about 0.3 % for  $f_{HDPE} \sim 5$  wt% (**Figure 32**). No estimate could be obtained for lower HDPE fractions since no SAXS scattering peak was recorded above the melting temperature of LDPE (cf. **Figure 23**). It should be noted that the Huang-Brown model does not consider trapped entanglements, which most likely also contribute to the creep resistance. Nilsson et al. have shown through numerical simulations that the number of trapped entanglements in polyethylene can be twice the number of tie chains<sup>139, 140</sup>.

One parameter that strongly influences the probability of tie-chain formation is the chain length. In an attempt to explore the impact of molecular weight the tie-chain probability was calculated for a variety of simulated resins with identical molecular-weight distributions but different  $M_w$ , which ranged from 4 to 2400 kg mol<sup>-1</sup> (see Paper V). To limit the number of variables, the same long period, lamellar thickness and PDI were used for all simulated resins, with values borrowed from

the LDPE/HDPE blend with  $f_{HDPE} = 5\text{wt}\%$  discussed in above (section 9.8). The probability of tie-chain formation increases rapidly from 0.01 to 0.4 % between  $10 \text{ kg mol}^{-1}$  and  $100 \text{ kg mol}^{-1}$ , and reaches a maximum of about 1% for  $M_w \geq 500 \text{ kg mol}^{-1}$  (Paper V).

**Table 2**, Summary of polyethylene blends comprising LDPE and HDPE or UHMW-PE: weight-fraction of HDPE  $f_{HDPE}$ ,  $M_w$  of the HDPE additive, total crystallinity  $X = \Delta H / \Delta H_f^0$ , and minimum stress  $\sigma_{fail}$  needed for creep fracture at  $115 \text{ }^\circ\text{C}$ .

| blend |         | $f_{HDPE}$<br>(wt%) | $M_w$<br>( $\text{kg mol}^{-1}$ ) | $X_c$<br>(%) | $\sigma_{fail}$<br>(kPa) |
|-------|---------|---------------------|-----------------------------------|--------------|--------------------------|
| LDPE  | HDPE    | 2                   | 4                                 | 49           | 1                        |
| LDPE  | HDPE    | 2                   | 16                                | 51           | 6                        |
| LDPE  | HDPE    | 2                   | 58                                | 51           | 8                        |
| LDPE  | HDPE    | 2                   | 99                                | 48           | 6                        |
| LDPE  | UHMW-PE | 2                   | 2400                              | 49           | 12                       |

To experimentally evaluate the impact of the HDPE chain length on the creep resistance above the melting temperature of LDPE, a series of blends were prepared that contained 2 wt% HDPE with  $M_w$  ranging from  $4 \text{ kg mol}^{-1}$  to  $2400 \text{ kg mol}^{-1}$  (**Table 2**). In order to quantify the creep resistance measurements were performed with a DMA. In a first set of experiments a constant creep stress of 1 kPa was applied to 1 mm thick samples at a constant temperature of  $115 \text{ }^\circ\text{C}$ . The creep was evaluated by comparing the strain after 60 min. LDPE fractured after  $\sim 35$  min. A blend containing low molecular-weight HDPE ( $4 \text{ kg mol}^{-1}$ ) fractured at  $\sim 50$  min. For all other samples creep was arrested when reaching a stable strain of 30-40%. In order to determine the creep stress that leads to fracture a series of creep experiments were carried out at a higher load (**Figure 33**). HDPE with a  $M_w$  of  $16 \text{ kg mol}^{-1}$  and  $100 \text{ kg mol}^{-1}$  fractured at 6 kPa. The HDPE grade of  $58 \text{ kg mol}^{-1}$  could sustain a slightly higher creep stress and fractured at 8 kPa. The increased ability to resist creep when using a HDPE with an intermediate molecular weight could be rationalised with a balance between tie-chain formation and co-crystallisation, both of which were found to increase with molecular weight (cf. Paper V). A blend containing 2 wt% UHMW-PE displayed the highest creep

resistance as evidenced by a significantly higher creep stress of 12 kPa that was required for fracture.

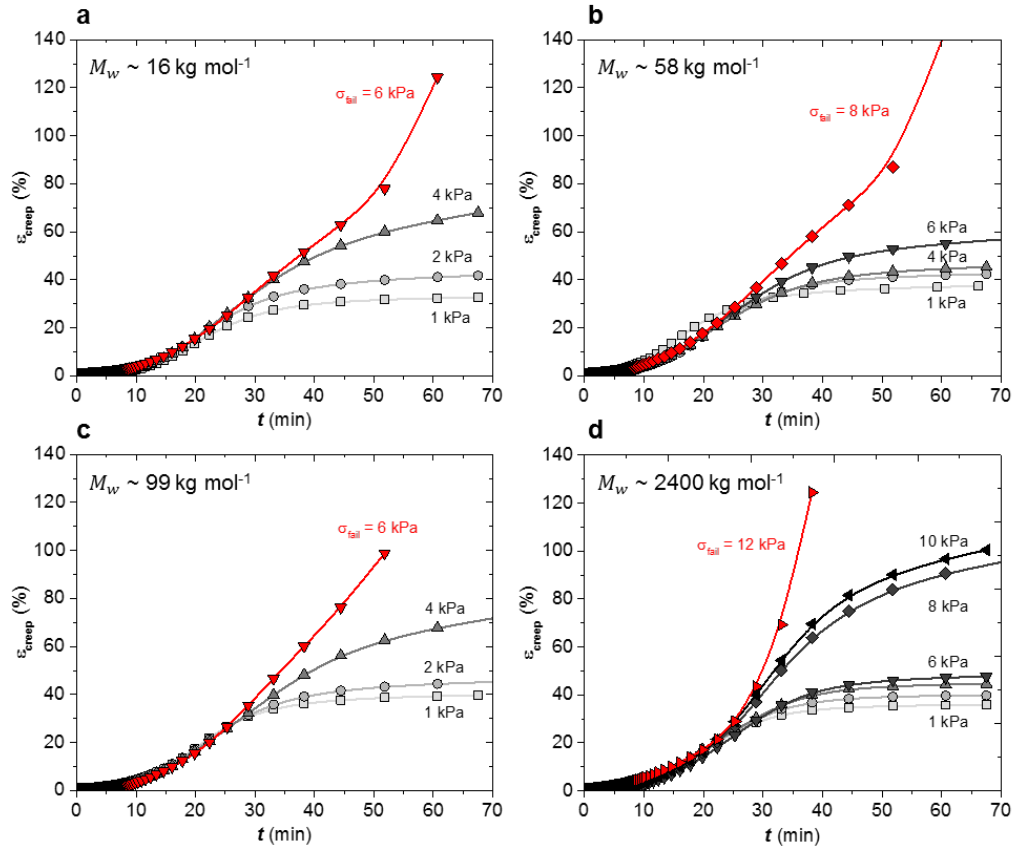


**Figure 33**, Creep strain  $\epsilon_{creep}$  at 115 °C and the indicated stress  $\sigma_{creep}$  for blends comprising LDPE and 2 wt% linear polyethylene with (a)  $M_w \sim 16 \text{ kg mol}^{-1}$ , (b)  $M_w \sim 58 \text{ kg mol}^{-1}$ , (c)  $M_w \sim 99 \text{ kg mol}^{-1}$ , and (d)  $M_w \sim 2400 \text{ kg mol}^{-1}$ ; the lowest stress  $\sigma_{fail}$  at which creep fracture occurred is shown in red.



# 10

## Conclusions

---

Two concepts of insulation material for high voltage cables have been presented, a nanocomposite and a polymer blend system. The nanocomposite contained 3 wt%  $\text{Al}_2\text{O}_3$  in LDPE and was tested as a benchmark and it was found to significantly decrease DC-conductivity. However the addition of nanoparticles had a negative effect on tree initiation voltage. In order to counter the low tree initiation voltage a thioxanthone voltage stabiliser was added. It was found that the attaching the voltage stabiliser to the surface of the nanoparticle did not improve the breakdown strength. However when the voltage stabiliser was mixed with the nanoparticle the breakdown strength was increased to the value of the original LPDE. Despite an increase in breakdown strength the conductivity of the nanocomposite could not be decreased rendering the addition of the stabiliser futile.

As an alternative to nanocomposites, blends of LDPE and HDPE were explored. An extensive material characterisation showed good miscibility of the blends in the melt. In the solid state a phase separated system containing homogeneously distributed HDPE crystals was found. An addition of 1-5 wt% HDPE was enough to significantly change the nanostructure of the blends and generate a fraction of thicker HDPE lamellae. The DC-conductivity of the tested blends were significantly decreased by approximately one order of magnitude for all blends. The improvement in conductivity could be a result of the increased amount of thicker lamellae introduced by HDPE. Breakdown measurements showed that the addition of a HDPE does not affect the tree initiation voltage.

The introduction of thicker lamellae have a significant impact on the thermomechanical properties of the blends. An addition of 2 wt% HDPE is sufficient to prevent creep at temperatures above the melting point for LDPE. The beneficial thermomechanical properties most likely originates from the formation of tie chains, which connects HDPE crystals through a network that retains the dimensions of the sample. The tie-chain probability for the blends was calculated by the Huang-Brown model using data from SAXS and DSC. A molecular weight dependence of the HDPE fraction on tie-chain probability and thermomechanical properties were also found.



# 11

## **The Future of insulation materials, author's thoughts**

---

It is clear that the insulation material has a vital role in the future energy grid that will transport green energy to our societies. There has been many attempts to improve the electrical, chemical and mechanical properties of the insulation material. Ranging from adding nanoparticles for a decreased conductivity, to voltage stabiliser for improving breakdown strength and new crosslinkers to ease the crosslinking process. Many of the attempts have led to valuable knowledge and has aided the research community to understand which processes and properties that are important when designing insulation materials. A hot topic has been nanoparticles, which has shown to improve electrical properties significantly when mixed in a polyethylene matrix. A large amount of studies on the nanocomposite system have been published during the last two decades. These studies have included different types of particles, different functionalisation, varying the size and shape of particles etc. The results displays a broad variation in the results, with a few common trends, such as lower conductivity and improved space charge distribution. In order to realise the nanocomposite concept as a high voltage cable insulation there are some issues that needs to be resolved. Many authors points to the interface between the polymer and the particle as one of the most important aspect. To take advantage of the high interface, particles needs to be well distributed and not aggregate. If particles aggregate it could lead to an inferior material. This is one of the difficulties in realising the full scale use of nanocomposites. To control the distribution of particles over thousands of meters insulation will be a challenge. The cost of creating such a process will most likely be expensive and questions arises if the benefits of using nanocomposites will outweigh the risk and price of the production.

In this thesis the concept of polymer blends has been discussed in detailed as an alternative to nanocomposites. It has been shown in this work that polyethylene blends can have similar effects on DC-conductivity as the nanocomposites, i.e. a decrease by one order of magnitude. However blends could be more beneficial for upscaling than nanocomposites, as they do not suffer the same distribution issues. By using thermoplastic blends of HDPE and LDPE the thermomechanical properties can be improved compared to neat LDPE. With this improvement the need for

crosslinking could be decreased or possibly eliminated completely. Although there seems to be several positive features of using polymer blends there are some issues to be addressed. For instance blends might be sensitive for temperature variations and annealing could change the nanostructure of the blends over time, which can affect the performance. The processes behind the improved electrical properties are not yet fully understood, therefore designing a reliable material could be puzzling. Regarding the mechanical aspects, a too stiff material might suffer from environmental stress cracking. The blends explored in this thesis were polyethylene based. However there is a range of other polymer blends that might be successful as insulation material. Recent reports have for instance suggested blending polypropylene with co-polymers of polyethylene and polypropylene to improve both mechanical strength and electrical properties. The way forward for high voltage insulation materials are not certain. Although nanocomposites promises a variety of improvements there seem to be uncertainties in the reliability and full scale production. On the other hand thermoplastic blends also displays promising electrical features but could be sensitive for temperature variations. Albeit there are issues to be solved in both concepts, the blend route seems to be the more feasible way considering an easier implementation and safer production. The research carried out within both of the concepts are central to expand the knowledge about the processes and mechanisms that controls the performance high voltage insulation.

# 12

## Acknowledgements

---

I want to thank the Swedish Foundation for Strategic Research, SSF (EM11-0022) for funding this project. I also want to thank Borealis AB in Stenungsund for supplying me with materials, doing electrical testing and most of all giving me expert help and guidance.

A very special thanks goes to Associate Professor Christian Müller, who has been my main supervisor. I cannot thank you enough for all the help, guidance, support and discussions that you gave me during these years. You have been an amazing supervisor and I am very grateful for having you guiding me through my PhD studies

I want to thank my Co-supervisor Professor Mats Andersson for accepting me as a PhD student in his group and for giving me support and motivation all the way from Adelaide.

My Co-supervisor Dr Thomas Gkourmpis, I want to thank you for all of the exciting discussions about science and of course also life in general. I also want to thank you for all the motivation you giving me, it has helped so much during the last year!

Dr Per-Ola Hagstrand I have really enjoyed all of our discussion during our meeting and the enthusiasm that you brought to this project. You are also responsible for starting the exciting work on the polymer blends which came to be the focus of this thesis.

A big thanks also goes to all the co-authors, especially Jonna Hynynen for putting in a lot of effort in experiments and thoughts on the polymer blends. I also want to acknowledge Carmen Cobo Sanches from KTH, I really enjoyed working with you all the days at KTH. Although not all experiments went as planned I had a great time and I appreciate all the discussions and hard work you put in our project.

The electrical measurements would not have been possible without the help from Professor Stanislaw Gubanski group. Thanks a lot for letting me use your high-voltage labs for treeing experiments and conductivity measurements and also for the sharing your expertise within the high voltage “field”. I want to acknowledge Assistant Professor Xiangrong Chen for the support during all the hours spent looking at growing trees, you made the hours pass fast with interesting discussions about high voltage and a lot of “other stuff”.

A big thanks goes to all the people that have helped with different experiments. Anders Mårtensson for SEM, GPC and FT-IR. Dr Anna Labrador, Dr Tomás Plivelic and Dr Sebastian Lages for assisting the SAXS measurements at MAXlab in Lund. Dr Toan Anh Hoang for DC-conductivity at Chalmers.

One of the most important contributions and the reason why this work was finished at all are all the colleagues and friends at Applied Chemistry and especially at floor eight. Without all the help, support, motivation, lunches, fikas, after works, festivities, training and etc, I would have quit a long a time ago. Having all these wonderful people around me has really made my time as a PhD student fantastic. There has been a lot of people coming and going and I want to thank a few former colleagues for all “interesting” discussions during fika and lunch, Markus Jarvid, Camilla Johansson, Zandra George, Anders Lennartsson and Sofie Gårdebjer. If you ever need your horoscope read just call me! Johnas Eklöf and David Kiefer thanks for all the lunches, discussions, travels, workouts and daily interruptions, it really have lighten up my days.

As I mentioned earlier all of the colleagues here at applied chemistry have been an amazing support and I would like to give an extra special thanks to all my colleagues in the Müller research group! I also want to thanks all my friend outside of Chalmers, with extra love to “ostkupan gänget”.

I want to thank my family, my mother, my father and my sister, for always giving me such an amazing support, love and always believing in me.

Finally I would like to thank Marie for always being there for me and supporting me. I love you!

## References

---

1. International Energy Agency: *Key World energy statistics*; 2016.
2. European Commission: *Energy roadmap 2050*; 2012.
3. DESERTEC: *Clean Power from Deserts, The DESERTEC Concept for Energy, Water and Climate Security*; 2007.
4. World Energy Council: *World Energy Resources*; 2013.
5. Energy Initiative Massachusetts Institute of Technology: *The Future of Solar Energy, An interdisciplinary MIT study*; 2015.
6. Andrews, D., The future of Electricity: Liberalisation, Long Distance Transmission, HVDC and Supergrids. <http://www.claverton-energy.com/>, 2009.
7. European Climate Foundation: *Roadmap 2050, practical guide to a prosperous, low-carbon Europe*; 2010.
8. Y. Murata; Sakamaki, M.; Abe, K.; Inoue, Y.; Mashio, S.; Kashiya, S.; Matsunaga, O.; Igi, T.; Watanabe, M.; Asai, S.; Katakai, S. *SEI TECHNICAL REVIEW* **2013**, (76).
9. Ryttoft, C.; Callavik, M.; Johansson, H.; Lundberg, P.; Jansson, E.; Bawa, H.; Funke, S.; Stoeter, S.; Moglestue, A. *60 years of HVDC*; 2014.
10. Mazzanti, G.; Marzinotto, M., *Extruded Cables for High-Voltage Direct-Current Transmission*. John Wiley & Sons: Hoboken, New Jersey, 2013.
11. Peschke, E.; Olshausen, R. V., *Cable Systems for High Voltage and Extra-High Voltage*. Publicis MCD Verlag: Munich, 1999.
12. Hanley, T. L.; Burford, R. P.; Fleming, R. J.; Barber, K. W. *IEEE Electrical Insulation Magazine* **2003**, 19, (1), 13-24.
13. Khalil, M. S. *IEEE Electrical Insulation Magazine* **1997**, 13, (6), 35-47.
14. Shen, Y. *DC Cable Systems With Extruded Dielectrics*; 2004.
15. Kuffel, E.; Zaengl, W. S.; Kuffel, J., *High Voltage Engineering: Fundamentals*. Elsevier Ltd.: Jordan Hill, Oxford, 2000.
16. Aoyama, H.; Matsui, K.; Tanaka, Y.; Takada, T.; Maeno, T., Observation and numerical analysis of space charge behavior in low-density polyethylene formed by ultra-high DC stress. In *Annual Report Conference on Electrical Insulation and Dielectric Phenomena (CEIDP)*, **2005**; 649-652.
17. Hayase, Y.; Matsui, K.; Tanaka, Y.; Takada, T.; Maeno, T., Packet-like charge behavior in various polyethylene. In *2007 Annual Report - Conference on Electrical Insulation and Dielectric Phenomena*, **2007**; 445-448.
18. Mizutani, T. In *High-voltage dc insulation and space charge*, Proceedings of the 6th International Conference on Properties and Applications of Dielectric Materials (Cat. No.00CH36347), **2000**; 18-23 vol.1.
19. Yewen, Z.; Lewiner, J.; Alquie, C.; Hampton, N. *IEEE Transactions on Dielectrics and Electrical Insulation* **1996**, 3, (6), 778-783.

## References

20. Fukagawa, H.; Imajo, T.; Sakamoto, Y. *IEEE Transactions on Power Apparatus and Systems* **1978**, PAS-97, (5), 1885-1892.
21. Gustafsson, A.; Saltzer, M.; Farkas, A.; Ghorbani, H.; Quist, T.; Jeroense, M. *The new 525 kV extruded HVDC cable system*; 2014.
22. *Elforsk Enmegavoltsutmaningen*; 2014.
23. Dissado, L. A.; Fothergill, J. C., *Electrical Degradation and Breakdown in Polymers*. P. Peregrinus: 1992.
24. Dissado, L. A. *IEEE Transactions on Dielectrics and Electrical Insulation* **2002**, 9, (4), 483-497.
25. Zhao, Y.; Vaughan, A. S.; Champion, J. V.; Dodd, S. J.; Sutton, S. J. In *The structure of electrical trees in semi-crystalline polymers*, 2000 Eighth International Conference on Dielectric Materials, Measurements and Applications (IEE Conf. Publ. No. 473), **2000**; 314-319.
26. Densley, R. J. *IEEE Transactions on Electrical Insulation* **1979**, EI-14, (3), 148-158.
27. Ieda, M.; Nawata, M. In *A consideration of treeing in polymers*, Conference on Electrical Insulation & Dielectric Phenomena - Annual Report 1972, **1972**; pp 143-150.
28. Chen, X.; Xu, Y.; Cao, X.; Dodd, S. J.; Dissado, L. A. *IEEE Transactions on Dielectrics and Electrical Insulation* **2011**, 18, (3), 847-860.
29. Bostrom, J. O.; Marsden, E.; Hampton, R. N.; Nilsson, U. *IEEE Electrical Insulation Magazine* **2003**, 19, (4), 6-12.
30. Khalil, M. S.; Gastli, A. *IEEE Transactions on Power Delivery* **1999**, 14, (3), 699-704.
31. Ashcraft, A. C.; Eichhorn, R. M.; Shaw, R. G. In *Laboratory studies of treeing in solid dielectrics and voltage stabilization of polyethylene*, IEEE International Conference on Electrical Insulation, **1976**; pp 213-218.
32. Davis, H. J., Electrical insulating composition based on polyolefin containing dye additives as voltage stabilizers. Google Patents: 1980.
33. Jarvid, M.; Johansson, A.; Bjuggren, J. M.; Wutzel, H.; Englund, V.; Gubanski, S.; Müller, C.; Andersson, M. R. *Journal of Polymer Science Part B: Polymer Physics* **2014**, 52, (16), 1047-1054.
34. Wutzel, H.; Jarvid, M.; Bjuggren, J. M.; Johansson, A.; Englund, V.; Gubanski, S.; Andersson, M. R. *Polymer Degradation and Stability* **2015**, 112, 63-69.
35. Jarvid, M.; Johansson, A.; Kroon, R.; Bjuggren, J. M.; Wutzel, H.; Englund, V.; Gubanski, S.; Andersson, M. R.; Müller, C. *Advanced Materials* **2015**, 27, (5), 897-902.
36. Patsch, R. *IEEE Transactions on Electrical Insulation* **1979**, EI-14, (4), 200-206.
37. Andrews, T.; Hampton, R. N.; Smedberg, A.; Wald, D.; Waschke, V.; Weissenberg, W. *IEEE Electrical Insulation Magazine* **2006**, 22, (6), 5-16.
38. Jarvid, M.; Johansson, A.; Englund, V.; Lundin, A.; Gubanski, S.; Müller, C.; Andersson, M. R. *Journal of Materials Chemistry A* **2015**, 3, (14), 7273-7286.
39. Osswald, T. A.; Baur, E.; Brinkmann, S.; Oberbach, K.; Schmachtenberg, E., *International Plastics Handbook - The Resource for Plastics Engineers (4th Edition)*. Hanser Publishers: 2006.

## References

40. Demirors, M., The History of Polyethylene. In *100+ Years of Plastics. Leo Baekeland and Beyond*, American Chemical Society: 2011; Vol. 1080, 115-145.
41. Larson, R. G.; Sridhar, T.; Leal, L. G.; McKinley, G. H.; Likhtman, A. E.; McLeish, T. C. B. *Journal of Rheology* **2003**, 47, (3), 809-818.
42. Bovey, F. A.; Schilling, F. C.; McCrackin, F. L.; Wagner, H. L. *Macromolecules* **1976**, 9, (1), 76-80.
43. Spěvák, J. *Polymer* **1978**, 19, (10), 1149-1152.
44. Soares, J. B. P.; McKenna, T. F. L., Introduction to Polyolefins. In *Polyolefin Reaction Engineering*, Wiley-VCH Verlag GmbH & Co. KGaA: 2012; 1-13.
45. Jung, M.; Lee, Y.; Kwak, S.; Park, H.; Kim, B.; Kim, S.; Lee, K. H.; Cho, H. S.; Hwang, K. Y. *Analytical Chemistry* **2016**, 88, (3), 1516-1520.
46. Doerpinghaus, P. J.; Baird, D. G. *Journal of Rheology* **2003**, 47, (3), 717-736.
47. Gedde, U. W., *Polymer Physics*. Springer Netherlands: 1999.
48. Peacock, A., *Handbook of Polyethylene: Structures: Properties, and Applications*. Taylor & Francis: 2000.
49. Blundell, D. J.; Beckett, D. R.; Willcocks, P. H. *Polymer* **1981**, 22, (5), 704-707.
50. Gray, A. P. *Thermochimica Acta* **1970**, 1, (6), 563-579.
51. Wunderlich, B.; Czornyj, G. *Macromolecules* **1977**, 10, (5), 906-913.
52. Glatter, O.; Kratky, O., *Small Angle X-ray Scattering*. Academic Press: London, 1982.
53. Keith, H. D.; Padden, F. J.; Vadimsky, R. G. *Science* **1965**, 150, (3699), 1026-1027.
54. Keith, H. D.; Padden, F. J.; Vadimsky, R. G. *Journal of Polymer Science Part A-2: Polymer Physics* **1966**, 4, (2), 267-281.
55. Seguela, R. *Journal of Polymer Science Part B: Polymer Physics* **2005**, 43, (14), 1729-1748.
56. Huang, Y.-L.; Brown, N. *Journal of Materials Science* **1988**, 23, (10), 3648-3655.
57. Huang, Y.-L.; Brown, N. *Journal of Polymer Science Part B: Polymer Physics* **1991**, 29, (1), 129-137.
58. Beveridge, C.; Sabiston, A. *Materials & Design* **1987**, 8, (5), 263-268.
59. Nilsson, S.; Hjertberg, T.; Smedberg, A. *European Polymer Journal* **2010**, 46, (8), 1759-1769.
60. Pearson, R. W. *Journal of Polymer Science* **1957**, 25, (109), 189-200.
61. Andersson, M. G.; Jarvid, M.; Johansson, A.; Gubanski, S.; Foreman, M. R. S.; Müller, C.; Andersson, M. R. *European Polymer Journal* **2015**, 64, 101-107.
62. Herman, J. N.; Biesenberger, J. A. *Polymer Engineering & Science* **1966**, 6, (4), 341-348.
63. Hittmair, P.; Ullman, R. *Journal of Applied Polymer Science* **1962**, 6, (19), 1-14.
64. Alemán, J.; Chadwick, A. V.; He, J.; Hess, M.; Horie, K.; Jones, R. G.; Kratochvíl, P.; Meisel, I.; Mita, I.; Moad, G.; Penczek, S.; Stepto, R. F. T. *Pure and Applied Chemistry* **2007**, 79, (10), 1801-1829.
65. Chawla, K. K., *Composite Materials*. Springer-Verlag New York: New York, 1998.
66. Jesson, D. A.; Watts, J. F. *Polymer Reviews* **2012**, 52, (3), 321-354.
67. Nelson, J. K., *Dielectric Polymer Nanocomposites*. Springer US: 2010.

## References

68. Lewis, T. J. *IEEE Transactions on Dielectrics and Electrical Insulation* **1994**, 1, (5), 812-825.
69. Wang, S. J.; Zha, J. W.; Wu, Y. H.; Ren, L.; Dang, Z. M.; Wu, J. *IEEE Transactions on Dielectrics and Electrical Insulation* **2015**, 22, (6), 3350-3356.
70. Hoang, A.; Pallon, L.; Liu, D.; Serdyuk, Y.; Gubanski, S.; Gedde, U. *Polymers* **2016**, 8, (3), 87.
71. Ishimoto, K.; Kanegae, E.; Ohki, Y.; Tanaka, T.; Sekiguchi, Y.; Murata, Y.; Reddy, C. C. *IEEE Transactions on Dielectrics and Electrical Insulation* **2009**, 16, (6), 1735-1742.
72. Pallon, L. K. H.; Olsson, R. T.; Liu, D.; Pourrahimi, A. M.; Hedenqvist, M. S.; Hoang, A. T.; Gubanski, S.; Gedde, U. W. *Journal of Materials Chemistry A* **2015**, 3, (14), 7523-7534.
73. Fleming, R. J.; Ammala, A.; Casey, P. S.; Lang, S. B. *IEEE Transactions on Dielectrics and Electrical Insulation* **2008**, 15, (1), 118-126.
74. Tian, F.; Lei, Q.; Wang, X.; Wang, Y. *IEEE Transactions on Dielectrics and Electrical Insulation* **2012**, 19, (3), 763-769.
75. Dongling, M.; Treese, A. H.; Richard, W. S.; Anna, C.; Eva, M.; Carina, Ö.; Linda, S. S. *Nanotechnology* **2005**, 16, (6), 724.
76. Hui, L.; Schadler, L. S.; Nelson, J. K. *IEEE Transactions on Dielectrics and Electrical Insulation* **2013**, 20, (2), 641-653.
77. Pourrahimi, A. M.; Hoang, T. A.; Liu, D.; Pallon, L. K. H.; Gubanski, S.; Olsson, R. T.; Gedde, U. W.; Hedenqvist, M. S. *Advanced Materials* **2016**, 28, (39), 8651-8657.
78. Pallon, L. K. H.; Hoang, A. T.; Pourrahimi, A. M.; Hedenqvist, M. S.; Nilsson, F.; Gubanski, S.; Gedde, U. W.; Olsson, R. T. *Journal of Materials Chemistry A* **2016**, 4, (22), 8590-8601.
79. Murata, Y.; Goshowaki, M.; Reddy, C. C.; Sekiguchi, Y.; Hishinuma, N.; Hayase, Y.; Tanaka, Y.; Takada, T. In *Investigation of space charge distribution and volume resistivity of XLPE/MgO nanocomposite material under DC voltage application*, International Symposium on Electrical Insulating Materials, **2008**; 502-505.
80. Wang, S.; Zha, J.; Wu, Y.; Yan, H.; Dang, Z. *American Journal of Engineering and Applied Sciences* **2015**, 8, (3), 405-409.
81. Alapati, S.; Thomas, M. J. *IEEE Transactions on Dielectrics and Electrical Insulation* **2012**, 19, (2), 697-704.
82. Han, B.; Wang, X.; Sun, Z.; Yang, J.; Lei, Q. *Applied Physics Letters* **2013**, 102, (1)
83. Tian, F.; Lei, Q.; Wang, X.; Wang, Y. *Applied Physics Letters* **2011**, 99, (14), 142903.
84. Lewis, T. J. *IEEE Transactions on Dielectrics and Electrical Insulation* **2004**, 11, (5), 739-753.
85. Nelson, J. K.; Hu, Y. *Journal of Physics D: Applied Physics* **2005**, 38, (2), 213.
86. Lewis, T. J. *IEEE Transactions on Dielectrics and Electrical Insulation* **2014**, 21, (2), 497-502.
87. Roy, M.; Nelson, J. K.; MacCrone, R. K.; Schadler, L. S.; Reed, C. W.; Keefe, R. *IEEE Transactions on Dielectrics and Electrical Insulation* **2005**, 12, (4), 629-643.

## References

88. Tanaka, T. *IEEE Transactions on Dielectrics and Electrical Insulation* **2005**, 12, (5), 914-928.
89. Zhang, W., Nanoparticle Aggregation: Principles and Modeling. In *Nanomaterial: Impacts on Cell Biology and Medicine*, Capco, D. G.; Chen, Y., Eds. Springer Netherlands: Dordrecht, 2014; pp 19-43.
90. Vaughan, A. S., Nanodielectrics: The Role of Structure in Determining Electrical Properties. In *Controlling the Morphology of Polymers: Multiple Scales of Structure and Processing*, Mitchell, G. R.; Tojeira, A., Eds. Springer International Publishing: Cham, 2016; pp 237-262.
91. Steennis, E. F.; Kreuger, F. H. *IEEE Transactions on Electrical Insulation* **1990**, 25, (5), 989-1028.
92. Liu, D.; Pourrahimi, A. M.; Olsson, R. T.; Hedenqvist, M. S.; Gedde, U. W. *European Polymer Journal* **2015**, 66, 67-77.
93. Cobo Sánchez, C.; Wåhlander, M.; Taylor, N.; Fogelström, L.; Malmström, E. *ACS Applied Materials & Interfaces* **2015**, 7, (46), 25669-25678.
94. Alemán, J. V.; Chadwick, A. V.; He, J.; Hess, M.; Horie, K.; Jones, R. G.; Kratochvíl, P.; Meisel, I.; Mita, I.; Moad, G.; Penczek, S.; Stepto, R. F. T., Definitions of terms relating to the structure and processing of sols, gels, networks, and inorganic-organic hybrid materials (IUPAC Recommendations 2007). In *Pure and Applied Chemistry*, 2007; Vol. 79, p 1801.
95. Flory, P. J. *The Journal of Chemical Physics* **1942**, 10, (1), 51-61.
96. Huggins, M. L. *The Journal of Physical Chemistry* **1942**, 46, (1), 151-158.
97. Scott, R. L. *The Journal of Chemical Physics* **1949**, 17, (3), 268-279.
98. Nwabunma, D.; Kyu, T., *Polyolefin Blends*. John Wiley & Sons Inc.: Hoboken, New Jersey, 2008.
99. Lohse, D. J. *Polym J* **2013**, 45, (1), 20-25.
100. Chen, J.-L.; Chang, F.-C. *Macromolecules* **1999**, 32, (16), 5348-5356.
101. Flory, P. J.; Eichinger, B. E.; Orwoll, R. A. *Macromolecules* **1968**, 1, (3), 287-288.
102. Shanks, R. A.; Li, J.; Yu, L. *Polymer* **2000**, 41, (6), 2133-2139.
103. Li, J.; Shanks, R. A.; Olley, R. H.; Greenway, G. R. *Polymer* **2001**, 42, (18), 7685-7694.
104. Teh, J. W.; Rudin, A.; Keung, J. C. *Advances in Polymer Technology* **1994**, 13, (1), 1-23.
105. Alamo, R. G.; Graessley, W. W.; Krishnamoorti, R.; Lohse, D. J.; Londono, J. D.; Mandelkern, L.; Stehling, F. C.; Wignall, G. D. *Macromolecules* **1997**, 30, (3), 561-566.
106. Zhao, L.; Choi, P. *Materials and Manufacturing Processes* **2006**, 21, (2), 135-142.
107. Cho, K.; Lee, B. H.; Hwang, K.-M.; Lee, H.; Choe, S. *Polymer Engineering & Science* **1998**, 38, (12), 1969-1975.
108. Barham, P. J.; Hill, M. J.; Keller, A.; Rosney, C. C. A., A Case for Liquid-Liquid Phase Segregation in Polyethylene Melts. In *Integration of Fundamental Polymer Science and Technology—3*, Lemstra, P. J.; Kleintjens, L. A., Eds. Springer Netherlands: Dordrecht, 1989; pp 291-295.
109. Hill, M. J.; Barham, P. J.; Keller, A.; Rosney, C. C. A. *Polymer* **1991**, 32, (8), 1384-1393.
110. Hill, M. J.; Barham, P. J. *Polymer* **1992**, 33, (19), 4099-4107.

## References

111. Hill, M. J.; Barham, P. J. *Polymer* **1992**, 33, (23), 4891-4897.
112. Hill, M. J.; Barham, P. J.; Keller, A. *Polymer* **1992**, 33, (12), 2530-2541.
113. Hill, M. J. *Polymer* **1994**, 35, (9), 1991-1993.
114. Hill, M. J.; Barham, P. J. *Polymer* **1995**, 36, (17), 3369-3375.
115. Wignall, G. D.; Londono, J. D.; Lin, J. S.; Alamo, R. G.; Galante, M. J.; Mandelkern, L. *Macromolecules* **1995**, 28, (9), 3156-3167.
116. Braña, M. T. C.; Gedde, U. W. *Polymer* **1992**, 33, (15), 3123-3136.
117. Xu, J.; Xu, X.; Chen, L.; Feng, L.; Chen, W. *Polymer* **2001**, 42, (8), 3867-3874.
118. Clampitt, B. H. *Journal of Polymer Science Part A: General Papers* **1965**, 3, (2), 671-679.
119. Lin, Y.; Du, W.; Tu, D.; Zhong, W.; Du, Q. *Polymer International* **2005**, 54, (2), 465-470.
120. Green, C. D.; Vaughan, A. S.; Stevens, G. C.; Sutton, S. J.; Geussens, T.; Fairhurst, M. J. *IEEE Transactions on Dielectrics and Electrical Insulation* **2013**, 20, (1), 1-9.
121. Vaughan, A. S.; Green, C. D.; Hosier, I. L.; Stevens, G. C.; Pye, A.; Thomas, J. L.; Sutton, S. J.; Geussens, T. In *Thermoplastic high performance cable insulation systems for flexible system operation*, 2015 IEEE Electrical Insulation Conference (EIC), **2015**; pp 543-546.
122. Kai, Z.; Lunzhi, L.; Lisheng, Z.; Liang, C.; Man, X.; Guanghui, C.; Mingli, F. In *DC dielectric properties of thermo-plastic polyolefin materials*, 2016 IEEE Conference on Electrical Insulation and Dielectric Phenomena (CEIDP), **2016**; pp 470-473.
123. Lunzhi, L.; Kai, Z.; Lisheng, Z.; Nan, C.; Man, X.; Darong, X.; Guanghui, C. In *Dielectric behaviors of recyclable thermo-plastic polyolefin blends for extruded cables*, 2015 IEEE 11th International Conference on the Properties and Applications of Dielectric Materials (ICPADM), **2015**; pp 180-183.
124. Hosier, I. L.; Vaughan, A. S.; Swinlger, S. G. *Journal of Polymer Science Part B: Polymer Physics* **2000**, 38, (17), 2309-2322.
125. Hoiser, I. L.; Vaughan, A. S.; Swinlger, S. G. *Journal of Materials Science* **1997**, 32, (17), 4523-4531.
126. *IEEE Std 930-2004 (Revision of IEEE Std 930-1987)* **2005**, 0\_1-41.
127. Labrador, A.; Cerenius, Y.; Svensson, C.; Theodor, K.; Plivelic, T. *J. Phys. Conf. Ser.* **2013**, 425, (7), 072019.
128. Adamec, V.; Calderwood, J. H. *Journal of Physics D: Applied Physics* **1981**, 14, (8), 1487.
129. Lau, K. Y.; Vaughan, A. S.; Chen, G.; Hosier, I. L.; Holt, A. F. *Journal of Physics: Conference Series* **2013**, 472, (1)
130. Chen, X.; Murdany, D.; Liu, D.; Andersson, M.; Gubanski, S. M.; Gedde, U. W.; Suwarno. *IEEE Transactions on Dielectrics and Electrical Insulation* **2016**, 23, (3), 1506-1514.
131. Das-Gupta, D. *IEEE Transactions on Dielectrics and Electrical Insulation* **1997**, 4, (2), 149-156.
132. Jose, N. M.-M.; Rodica, M. N.; Eugen, R. N. *Journal of Physics D: Applied Physics* **2004**, 37, (3), 343.
133. Montanari, G. C.; Mazzanti, G.; Palmieri, F.; Motori, A.; Perego, G.; Serra, S. *Journal of Physics D: Applied Physics* **2001**, 34, (18), 2902.

## References

134. Zhou, F.; Li, J.; Liu, M.; Min, D.; Li, S.; Xia, R. *IEEE Transactions on Dielectrics and Electrical Insulation* **2016**, 23, (2), 1174-1182.
135. Poole, H. H. *Philosophical Magazine Series 6* **1916**, 32, (187), 112-129.
136. Wintle, H. J. *IEEE Transactions on Dielectrics and Electrical Insulation* **1999**, 6, (1), 1-10.
137. Ping, Y.; Ynanxiang, Z.; Guansheng, S.; Yoshimura, N. In *Influence of morphology and thermal stability on tree initiation in polyethylene films*, 2001 Annual Report Conference on Electrical Insulation and Dielectric Phenomena, **2001**; pp 249-252.
138. Smedberg, A.; Boström, J.-O.; Wald, D.; Peters, R., Comparison of different Analytical Test Methods to Monitor Crosslinking By-products in XLPE Insulated Cables. In *Jicable*, Paris-Versailles, 2007.
139. Nilsson, F.; Lan, X.; Gkourmpis, T.; Hedenqvist, M. S.; Gedde, U. W. *Polymer* **2012**, 53, (16), 3594-3601.
140. Moyassari, A.; Mostafavi, H.; Gkourmpis, T.; Hedenqvist, M. S.; Gedde, U. W.; Nilsson, F. *Polymer* **2015**, 72, 177-184.